Nanotechnology, Science and Applications

Dovepress
Taylor & Francis Group

Open Access Full Text Article

ORIGINAL RESEARCH

Paclitaxel-Loaded Polyelectrolyte Nanocarriers: Uptake Mechanisms, Cytotoxicity, and Genotoxicity in Human Endothelial and Breast Cancer Cells

Marzena Szwed[1], Anastazja Poczta-Krawczyk[1], Katarzyna Dominika Kania[2,3], Karol Bukowski[1], Katarzyna Bednarska-Szczepaniak[4], Agnieszka Marczak[1], Krzysztof Szczepanowicz[5]

[1]Department of Medical Biophysics, Institute of Biophysics, Faculty of Biology and Environmental Protection, University of Lodz, Lodz, 90-236, Poland; [2]Laboratory of Virology, Institute of Medical Biology, Polish Academy of Sciences, Lodz, 93-232, Poland; [3]Department of Diagnostic Techniques in Pathomorphology, Medical University of Lodz, Lodz, 92-213, Poland; [4]Laboratory of Medicinal Chemistry, Institute of Medical Biology, Polish Academy of Sciences, Lodz, 92-232, Poland; [5]Jerzy Haber Institute of Catalysis and Surface Chemistry, Polish Academy of Sciences, Kraków, 30-239, Poland

Correspondence: Marzena Szwed, Department of Medical Biophysics, Institute of Biophysics, Faculty of Biology and Environmental Protection, University of Lodz, Pomorska 141/143 St, Lodz, 90-236, Poland, Email marzena.szwed@biol.uni.lodz.pl

Purpose: This study explores the therapeutic potential of sodium dodecyl sulphate (SDS)-based nanocarriers (NCs) for the targeted delivery of paclitaxel (PTX) to breast cancer (BC) cells, with a particular focus on the mechanisms governing their intracellular transport and biological activity.

Methods: Two types of SDS-based NCs differing in polyelectrolyte composition: poly-L-lysine (SDS/PLL) and poly-L-lysine with poly-L-glutamic acid (SDS/PLL/PGA), were prepared following the Layer-by-Layer (LbL) technique. Cellular uptake and distribution of Rhodamine B (RhoB)-labelled NCs were assessed via fluorescence microscopy and quantified by flow cytometry across three human cell lines: dermal microvascular endothelial cell line (HMEC-1), epithelial breast adenocarcinoma cell line (MCF-7), and triple-negative, mesenchymal-like BC cell line (MDA-MB-231). The cytotoxic and genotoxic effects of PTX-loaded NCs were evaluated using spectrophotometric and spectrofluorimetric assays. In parallel, DNA damage-responsive gene expression was examined by quantitative real-time reverse transcription polymerase chain reaction (qRT-PCR).

Results: Both NC formulations demonstrated comparable uptake efficiency, despite differences in fluorescence intensity. Inhibitor-based studies revealed distinct internalization pathways: SDS/PLL NCs entered via dynamin-dependent endocytosis and macropinocytosis, whereas SDS/PLL/PGA NCs relied predominantly on macropinocytosis. Genotoxicity of PTX-loaded NCs was confirmed by comet assay and H2A histone family member X (γH2AX) phosphorylation, particularly in MCF-7 and MDA-MB-231 cells. Cell cycle perturbations and transcriptional changes in ataxia-telangiectasia mutated (*ATM*), ATM and Rad3-related (*ATR*), and cyclin-dependent kinase 1 (*CDK1*) genes accompanied these effects. Enzyme-linked immunosorbent assay (ELISA)-based analyses further demonstrated apoptosis-mediated cytotoxicity induced by both investigated formulations.

Conclusion: These findings delineate the cellular uptake mechanisms and in vitro biological effects of the examined polyelectrolyte NCs for PTX delivery, with a particular focus on their genotoxicity. Collectively, these in vitro data provide a mechanistic basis to inform the rational design and preclinical optimization of SDS-based NCs, supporting subsequent in vivo evaluation.

Keywords: nanoparticles, taxanes, layer-by-layer technique, breast cancer

Introduction

By 2050, annual cancer incidence is projected to approach ~35 million cases. In 2022, there were ~20 million new diagnoses and 9.7 million deaths worldwide. Breast cancer accounted for about 2.3 million new cases in women and 670,000 deaths that year. It remains the most frequently diagnosed cancer in women and a leading cause of cancer

Received: 5 September 2025
Accepted: 22 November 2025
Published: 24 December 2025

mortality. This sustained burden supports the need for safer, more selective systemic treatments and mechanistically informed drug-delivery strategies for breast cancer.[1]

Conventional chemotherapy based on low-molecular-weight anticancer agents, such as anthracyclines and taxanes, remains one of the primary treatment modalities for both pre-invasive and invasive breast cancer (BC).[2,3] However, this therapeutic approach is associated with high systemic toxicity and poor selectivity towards tumour cells. As a result, insufficient drug accumulation within the tumour microenvironment is often accompanied by significant toxicity to healthy tissues.[4] Rapidly proliferating cells, particularly those of the bone marrow tissue and gastrointestinal epithelium, are especially vulnerable to the adverse effects of these highly cytotoxic therapeutic agents.[5] To address these limitations, drug carriers are increasingly employed in chemotherapy to deliver cytotoxic agents at high concentrations specifically to cancer cells, while sparing normal tissues.[6] The concept of drug delivery systems (DDS) originates from Paul Ehrlich's early 20th-century "magic bullet" hypothesis.[7] According to this paradigm, an ideal drug carrier should: (1) enable optimal drug accumulation and release within the tumour niche; (2) exhibit an extended half-life in systemic circulation; and (3) display minimal toxicity towards non-cancerous tissues. In essence, the therapeutic effect should be restricted exclusively to malignant cells, leaving healthy tissues unaffected.[7]

Nanoparticles (NPs), a product of nanotechnology, have rapidly gained recognition as effective vehicles for drug delivery. Due to their unique properties (a large specific surface area relative to their mass and high reactivity), NPs may be applied during chemotherapy for various types of cancer.[8] The application of DDS in chemotherapy is further supported by the structural characteristics of the tumour microenvironment, where intercellular gaps are estimated to range from approximately 100 to 800 nm. However, in healthy tissues, the distance of these spaces is only about 2 nm.[9] Taking advantage of this difference, it has been found that nanocarriers (NCs) can freely enter and easily accumulate within the tumour niche.[10,11] Moreover, a phenomenon known as the enhanced permeability and retention effect may serve as an additional factor supporting the application of NPs in BC therapy. Currently, the scientific literature describes various nanovehicles whose primary function is to deliver therapeutic substances to cancer cells.[12]

A unique group of DDS comprises polyelectrolyte-based NCs, which dissociate into polyanions and polycations in aqueous solutions.[13,14] Many biomacromolecules, such as nucleic acids, proteins, or polysaccharides, are polyelectrolytes.[15] The use of polyelectrolytes in the preparation of NCs is highly desirable, as they can increase the biocompatibility of nanosystems and prolong their half-life in the human body.[16] It has been previously reported that NPs suspensions in body fluids tend to aggregate rapidly.[17] This phenomenon is attributed to differences in ionic strength between particles and body fluids, or the adsorption of serum proteins by the administered nanomaterials.[18] Therefore, to minimize the risk of undesirable nanocarrier–biological fluid interactions, the surfaces of nanomaterials are coated with hydrophilic, flexible, and non-ionic polyelectrolyte polymers. Polyelectrolytes such as poly-L-amino acids, eg, poly-L-lysine (PLL) and poly-L-glutamic acid (PGA), exhibit properties similar to those of biomacromolecules and dissociate readily in aqueous solutions. Consequently, they have been successfully used to produce biodegradable polymer NCs through sequential Layer-by-Layer (LbL) adsorption of oppositely charged polyelectrolytes.[19,20]

Sukhorukov's group made a significant contribution to research on the LbL technique,[21] who employed this method to form polyelectrolyte multilayers on colloidal particles. Moreover, the colloidal particles may either contain the active ingredient or serve as the core of the capsule.[22,23] The multifunctionality of NCs synthesised via the LbL technique can be exploited in two types of DDS: (1) passive targeting, in which specific modifications to the polyelectrolyte coating extend the NCs' circulation time in the body; and (2) active targeting, which requires the incorporation of targeting ligands, such as those that bind to specific cell surface receptors.[24]

Recently, the LbL method for forming multilayer-coated capsules has been extended to other types of cores,[25] including liquid cores.[26,27] Nanoemulsions are a special type of liquid-core NCs, produced by the saturation method, in which an active substance is encapsulated within a liquid core. During the LbL process, surfactants may be applied, which, together with oppositely charged polyelectrolytes, form a single core nanocapsule. NCs containing a liquid-core nanoemulsion of the oil-in-water type, stabilized with a cationic surfactant such as docusate sodium salt or dioctadecyldimethylammonium bromide, have been well characterized by Szczepanowicz et al.[28]

Recent studies have shown that biodegradable NCs stabilized by docusate sodium salt and PLL can be used to deliver hydrophobic, phase-soluble compounds.[29] However, cationic, oil-permeable surfactants have thus far been exclusively

soluble in highly toxic organic solvents, such as alcohols, haloalkanes, ethers, and ethylene glycol esters, which have raised significant concerns regarding their use in the synthesis of NCs via the LbL method.

We recently described a new method for synthesizing polyelectrolyte multicore NCs for hydrophobic drugs, based on the water-soluble surfactant sodium dodecyl sulphate (SDS).[19,20] The applicability of these SDS-based multicore NCs as DDS for paclitaxel (PTX) was evaluated using a comprehensive panel of in vitro assays, including viability and proliferation tests, analysis of cellular morphology, mitochondrial homeostasis disturbance, and cell death induction, conducted on BC cell lines. Two forms of polyelectrolyte multicore NCs were tested: one coated with PLL (SDS/PLL) and the other further coated with PGA (SDS/PLL/PGA).[19] Besides, cytotoxicity evaluation of SDS-based NCs loaded with PTX performed on HL-1 mouse cardiomyocytes showed that, among the tested NCs, SDS/PLL/PGA/PTX triggered less cellular stress in cardiac cells compared to SDS/PLL/PTX or PTX alone. The observed decrease in cardiotoxicity was attributed to a lower reduction in cellular viability and diminished mitochondrial damage.[20]

Although we observed similar anticancer properties for free PTX and PTX encapsulated into SDS-based NCs, the intracellular transport mechanism of highly hydrophobic drugs encapsulated in these NCs remains largely unexplored. In most tumour tissues, clathrin-mediated endocytosis (CME) and caveolin-mediated endocytosis are the primary pathways involved in the cellular uptake of NPs.[30] Typically, intracellular drug release from NPs occurs either through carrier degradation or drug diffusion. However, the mechanisms by which PTX-loaded NCs are internalized by different types of malignant and non-malignant cells remain poorly understood.

Despite extensive progress in nanomedicine, how polyelectrolyte nanocarriers' physicochemical attributes map onto cell-type-specific uptake routes and downstream DNA damage responses (DDR) remains incompletely defined. Size and surface charge are known to bias entry via clathrin-mediated endocytosis, caveolar pathways, or macropinocytosis, yet whether these routes condition intracellular trafficking, drug release kinetics, and genotoxic outcomes has been less systematically compared across endothelial versus breast cancer cells. Notably, endothelial cells are particularly rich in caveolae owing to high caveolin-1 (Cav-1) abundance. In contrast, breast cancer lines display heterogeneous Cav-1 expression across subtypes, which is commonly higher in triple-negative models than in luminal A cells. This supports the expectation of distinct distributions of endocytic routes between these cell types.[31–33] Therefore, as a mechanistic follow-up to our platform reports on SDS-derived polyelectrolyte carriers[34] we investigated both the uptake profile and endocytic mechanisms of these nanocarriers in HMEC-1, MCF-7, and MDA-MB-231, and their molecular consequences, including DNA damage and induction of programmed cell death, using DDR readouts (comet assay, γH2AX, PARP) under PTX exposure (Figure 1A and B).

To determine whether the mode of transport of the investigated SDS-based multicore NCs differs in a cell type-dependent manner, experiments were performed on dermal microvascular endothelial cell line (HMEC-1), epithelial breast adenocarcinoma cell line (MCF-7), and triple-negative, mesenchymal-like BC cell line (MDA-MB-231). For uptake tracking, the NCs were labelled with Rhodamine B (RhoB). Notably, the use of a panel of endocytosis inhibitors enabled us to identify the specific internalization pathways involved in NCs transport.

Given that PTX is a well-established anticancer agent with strong cytostatic properties, we also aimed to assess whether the SDS-based NC formulations retained their genotoxic potential. Three complementary techniques: spectrofluorimetry, spectrometry, and quantitative real-time reverse transcription polymerase chain reaction (qRT-PCR) were used. In parallel, we evaluated the pro-apoptotic and antiproliferative activity of SDS-based multicore NCs loaded with PTX. Finally, we analyze the consistency of the anticancer properties of the investigated NCs alongside their intracellular accumulation.

Materials and Methods

Materials

SDS, PLL hydrobromide (MW ~15,000–30,000), PGA sodium salt (MW ~15,000–50,000), and lissamine RhoB sulfonyl chloride were purchased from Sigma-Aldrich Chemie GmbH (Germany). PTX was supplied by Selleckchem (USA), while absolute ethanol was sourced from Avantor Performance Materials (Gliwice, Poland). The rhodamine-labelled poly-L-lysine (PLL/RhoB) was synthesised following the protocol described in Bioconjugate Techniques.[35] Distilled

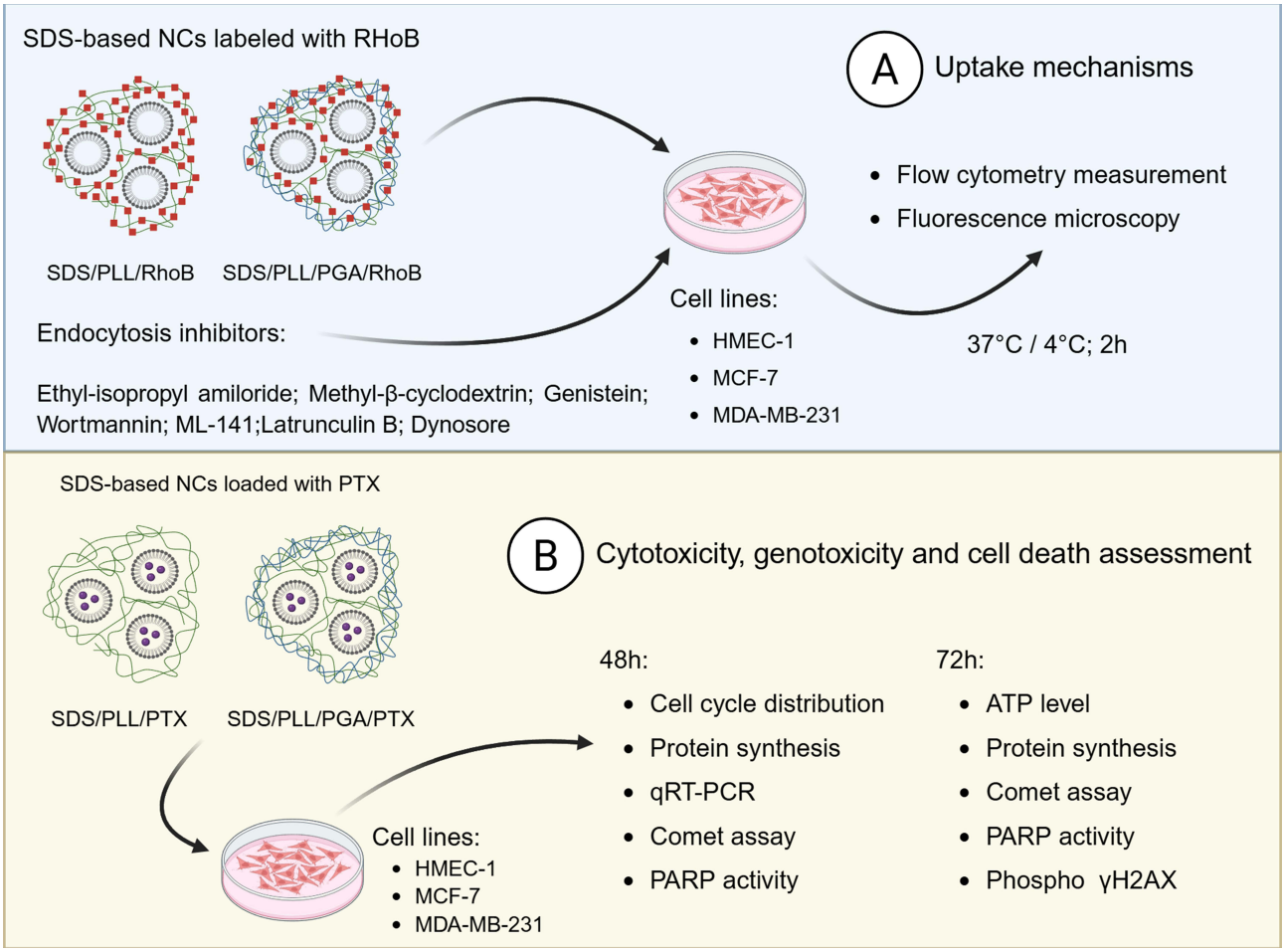

Figure 1 Overview of the experimental workflow. (**A**) Schematic representation of the experimental setup used to investigate the uptake mechanisms of SDS/PLL/RhoB and SDS/PLL/PGA/RhoB NCs in HMEC-1, MCF-7, and MDA-MB-231 cells. To optimize experimental conditions, the fluorescence of the cells was initially assessed in media supplemented with varying concentrations of fetal bovine serum (FBS; 1% or 10%). Subsequently, a comprehensive panel of endocytosis inhibitors was used to identify the pathways involved in the internalization of multicore SDS-based NCs. (**B**) Outline of the analytical approach used to compare the genotoxic and pro-apoptotic effects of PTX encapsulated in SDS/PLL and SDS/PLL/PGA NCs, relative to the cytotoxicity of the free drug. Created in BioRender Marczak, A. (2025) https://BioRender.com/om9tuhn.

water for all solvent and buffer preparations was obtained using a Millipore Direct-Q 5UV purification system (Merck Millipore, Darmstadt, Germany). Dulbecco's Modified Eagle Medium (DMEM), streptomycin, penicillin, trypsin–EDTA, sodium chloride (NaCl), low-melting-point agarose, normal-melting-point agarose, Triton X-100, 4′,6-diamidino-2-phenylindole (DAPI), hydrogen peroxide (H_2O_2), propidium iodide (PI), RNase A, trypan blue, RhoB, TriPure™ Isolation Reagent, endocytosis inhibitors, Hoechst 33258, and primers for qRT-PCR were purchased from Sigma-Aldrich (St. Louis, MO, USA). MCDB medium, hydrocortisone, and glutamine were obtained from the American Type Culture Collection (ATCC, Manassas, VA, USA). Phosphate-buffered saline (PBS), FBS, epidermal growth factor (EGF), and the High-Capacity cDNA Reverse Transcription Kit were acquired from Thermo Fisher Scientific (Waltham, MA, USA). The PARP Universal Colorimetric Assay Kit and Human Phospho-Histone γH2AX (S139) DuoSet IC ELISA Kit were purchased from R&D Systems (Minneapolis, MN, USA). Additional reagents included the CellTiter-Glo® Luminescent Cell Viability Assay (Promega, Madison, WI, USA), the Protein Synthesis Assay Kit (Green, ab239725; Abcam, Cambridge, UK), the MycoAlert™ Mycoplasma Detection Kit (Lonza, Walkersville, MD, USA), SYBR Green I Master Mix (Roche Holding AG, Basel, Switzerland), and PTX (Selleck Chemicals, Houston, TX, USA). Absolute ethanol was purchased from Avantor Performance Materials (Gliwice, Poland). All other chemicals and solvents were obtained from Sigma-Aldrich (St. Louis, MO, USA) or Avantor Performance Materials Poland S.A. (Gliwice, Poland).

Cells and Treatments

HMEC-1, MCF-7, and MDA-MB-231 were obtained from the ATCC (Manassas, VA, USA). HMEC-1 cells were cultured in MCDB medium supplemented with 10% (v/v) FBS, 100 µg/mL streptomycin, 100 U/mL penicillin, 10 ng/mL EGF, 1 µg/mL hydrocortisone, and 10 mM glutamine. MCF-7 and MDA-MB-231 cells were maintained in DMEM supplemented with 10% (v/v) FBS, 100 µg/mL streptomycin, and 100 U/mL penicillin.

All cells were cultured at 37 °C in a humidified incubator with a 5% (v/v) CO_2 atmosphere and routinely screened for mycoplasma contamination using the MycoAlert™ Mycoplasma Detection Kit. The trypan blue exclusion assay was used to assess cell viability and determine doubling time and growth rate, ensuring exponential proliferation and viability above 90%. Cells were seeded 24 hours before treatment with the tested compounds. Cell density and culture volume were adjusted according to the specific requirements of each experimental method. PTX and SDS-based NCs, whether empty or PTX-loaded, were diluted in culture medium with NaCl (0.9% w/v) as the solvent, as appropriate. All assays included a negative control (untreated cells). PTX and PTX-loaded nanocarriers were applied at final PTX concentrations of 12.5, 25, and 50 nM across all assays unless otherwise indicated; vehicle controls matched the highest solvent content.

Preparation and Physicochemical Characterisation of Polyelectrolyte Multicore Nanocarriers

Polyelectrolyte multicore NCs were synthesised through electrostatic self-assembly employing the LbL technique, following the procedure detailed in patent claim WIPO ST 10/C PL443843. Briefly, nanocores were formed by adding the water-soluble surfactant SDS (at 10× its critical micelle concentration) to a solution of PLL or PLL/RhoB (200 ppm in 0.015 M NaCl) under gentle magnetic stirring. These positively charged multicores NCs were then further coated with the polyanion, PGA, using the LbL saturation method by adding the SDS/PLL (or SDS/PLL/RhoB) nanocore dispersion to a PGA solution (2000 ppm). A critical optimisation step for both core formation and polyanion coating involved systematically determining the optimal SDS-to-PLL (or SDS-to-PLL/RhoB) and SDS/PLL-to-PGA (or SDS/PLL/RhoB-to-PGA) ratios. These ratios were selected using the saturation method of LbL assembly, by gradually increasing the amount of each component until a reversal in surface charge was observed, followed by stabilization of the zeta potential at a constant value, indicating complete surface coverage and electrostatic equilibrium. Colloidal stability assessments further supported this optimisation. For the encapsulation of PTX (61 mg/mL), the anticancer agent was initially solubilized in SDS micelles with the aid of absolute ethanol, which was then evaporated before the SDS/PLL or SDS/PLL/RhoB nanocores were formed. The particle size, size distribution, polydispersity index (PDI), and zeta potential of the samples were analysed using Dynamic Light Scattering and electrophoretic light scattering with a Zetasizer Nano ZS (Malvern-Panalytical Ltd., Malvern, UK). All measurements were performed at 25 °C in 0.015 M NaCl, with results averaging over a minimum of three independent runs, each consisting of 10 individual measurements. The temporal stability of the multicore nanocarriers was assessed by visual inspection at ambient temperature (monitoring for precipitation, flocculation/opalescence, and phase separation); all nanocarriers used in biological assays were freshly synthesised.

In parallel, to verify the labelling efficiency of SDS/PLL and SDS/PLL/PGA NCs with RhoB, the fluorescence intensity of the prepared capsules was measured using a Fluoroskan Ascent microplate reader (Labsystems, Sweden) with excitation and emission filter pairs of 530 nm and 590 nm, respectively.

Cytotoxicity – ATP Assay

Intracellular ATP levels were quantified using the CellTiter-Glo® Luminescent Cell Viability Assay (Promega, Madison, USA), following the manufacturer's protocol.[20] The experimental conditions included: untreated cells (negative control), cells treated with NaCl solution (0.9% w/v), empty NCs, PTX-loaded NCs, or PTX-loaded NCs labelled with RhoB. Cells were seeded in 96-well transparent plates and incubated with the respective compounds for up to 72 h under standard culture conditions (37 °C, 5% CO_2). Following incubation, half of the culture medium was replaced with an equal volume of the CellTiter-Glo reagent and gently mixed for 10 min at room temperature. The resulting lysates were

transferred to 96-well white plates, and luminescence was measured using a Fluoroskan Ascent FL microplate reader (Labsystems, Sweden) and expressed as relative luminescence units.

Protein Synthesis Assay

Alterations in protein synthesis were quantified using the Protein Synthesis Assay Kit – Green (Abcam, Cambridge, UK), following the manufacturer's instructions. Cells were preincubated with SDS-based NCs loaded with PTX or free PTX for 48 and 72 h at 37 °C. After fixation and permeabilisation, the culture medium was replaced with fresh medium containing the fluorescent protein label, and cells were incubated for 30 min at room temperature in the dark. Subsequently, cells were centrifuged, washed, and resuspended in PBS. Nuclear DNA was then stained using Hoechst 33258. Green and blue fluorescence, corresponding to newly synthesised proteins and nuclear DNA, respectively, was measured using a Fluoroskan Ascent FL microplate reader (Labsystems, Sweden).

Intracellular Accumulation of SDS-Based Nanocapsules

Intracellular accumulation of SDS-based NCs was measured by flow cytometry based on the red fluorescence of RhoB-labelled NCs. Following 2 h of incubation at 37 °C with RhoB-labelled NCs, cells were washed with PBS, harvested using trypsin, pelleted by centrifugation (*400* × *g*), resuspended in PBS, and analysed by flow cytometry within 30 minutes. RhoB fluorescence was detected using the phycoerythrin (PE) channel on a BD LSR II flow cytometer (BD Biosciences, Franklin Lakes, NJ, USA). To assess the impact of FBS concentration on intracellular accumulation, cells were incubated with NCs in medium supplemented with either 1% or 10% FBS for 2 hours at 37 °C. To confirm that the detected fluorescence signal originated from intracellular, endocytosed NCs rather than from membrane-bound particles, a parallel experiment was conducted under identical conditions but at 4 °C (instead of 37 °C), where energy-dependent endocytosis is suppressed.

Endocytosis Inhibitor Studies

Endocytosis inhibition experiments were performed following 24 h of cell growth in 24-well plates (5000 cells/well). Cells were preincubated with specific endocytosis inhibitors for 30 min at 37 °C, followed by treatment with RhoB-labelled NCs for 2 h in Roswell Park Memorial Institute (RPMI) medium supplemented with 1% FBS. Details for each endocytosis inhibitor (compound name, final in-well concentration, molecular function/target, catalogue number, and reference) are summarized in Supplementary Table 1. After incubation, cells were washed with PBS, harvested using trypsin, pelleted by centrifugation (*400* × *g*), resuspended in PBS, and prepared for flow cytometric analysis. Fluorescence was measured using the PE channel on an LSR II flow cytometer (BD Biosciences, Franklin Lakes, NJ, USA).

Cell Cycle Analysis

Cellular DNA content was assessed by flow cytometry using PI staining. HMEC-1, MCF-7, and MDA-MB-231 cells were treated for 48 hours with free PTX, SDS/PLL/PTX, or SDS/PLL/PGA/PTX. Following treatment, the cells were harvested, washed with PBS, fixed in ice-cold 70% ethanol, and stored at −20 °C. Before staining, cells were washed, resuspended in fresh PBS, and allowed to equilibrate to ambient temperature (20–22 °C). Samples were then incubated for 30 minutes at 37 °C in a staining solution containing 0.05 mg/mL PI and 0.02 mg/mL RNase A in PBS. DNA content and cell cycle distribution were analysed using a Becton Dickinson FACS LSR II cytometer (BD Biosciences), with excitation at 488 nm and detection of red fluorescence in the FL3 channel. Each experiment was performed in triplicate. Cell populations in distinct cell cycle phases were quantified from standard counts of 10,000 events using Flowing Software (University of Turku, Finland).

Comet Assay

To evaluate the impact of the tested compounds on DNA damage in the examined cell lines, the alkaline version of the comet assay (pH > 13) was performed. The procedure followed the protocol of Singh et al[36] with minor modifications. Cells were treated with PTX, SDS/PLL/PTX, or SDS/PLL/PGA/PTX for 48 and 72 hours. As a positive control, cells

were exposed to 100 µM H_2O_2 for 10 minutes at 4 °C. Following electrophoresis and DAPI staining, the slides were analysed using an Eclipse fluorescence microscope (Nikon, Tokyo, Japan) at 200× magnification, coupled to a COHU 4910 video camera (Cohu, Inc., San Diego, CA) equipped with a UV filter block and connected to the Lucia-Comet v.4.51 image analysis system (Laboratory Imaging, Prague, Czech Republic). For each sample, fifty nuclei were randomly selected and analysed. The percentage of DNA in the comet tail was used as the index of DNA damage, with the mean value reported per sample.

PARP Assay

Poly(ADP-ribose) polymerase (PARP) activity was determined after 48 and 72 hours of incubation with free PTX, SDS/PLL/PTX, or SDS/PLL/PGA/PTX NCs using the PARP Universal Colorimetric Assay Kit, according to the manufacturer's instructions (Thermo Fisher Scientific Inc., Waltham, MA, USA). Following treatment, cells were washed with PBS, lysed, and the resulting clarified extracts were used to evaluate PARP enzymatic activity. Detection of the histone - ATP - biotin complex was achieved through the addition of tetramethylbenzidine. Absorbance was measured at 650 nm using a BioTek Microplate Reader (Winooski, VT, USA).

γH2AX Assay

To evaluate the level of H2A histone family member X (γH2AX) phosphorylated at Ser139 in the examined cells following 48- and 72-hour treatments with PTX, SDS/PLL/PTX, or SDS/PLL/PGA/PTX at 50 nM, the Human Phospho-Histone γH2AX (Ser139) DuoSet IC ELISA Assay Kit (RayBiotech, Norcross, GA, USA) was used. All procedures were performed following the manufacturer's instructions. After treatment, cells were permeabilised and incubated with a rabbit monoclonal primary antibody specific for phospho-γH2AX (Ser139) at a 1:100 dilution, followed by an anti-rabbit secondary antibody at a 1:1000 dilution. Fluorescence was measured using a Fluoroskan Ascent plate reader (Fluoroskan Ascent FL, Stockholm, Sweden) equipped with filter pairs 540/600 nm and 360/450 nm. Results are expressed as the ratio of phosphorylated γH2AX (540/600 nm) to total histone γH2AX (360/450 nm).

Quantitative Real-Time PCR

Following 48-hour incubation with PTX or PTX encapsulated in multicore SDS-based NCs, total RNA was extracted using TriPure™ Isolation Reagent following the manufacturer's protocol (Sigma-Aldrich, St. Louis, MO, USA). RNA concentration and integrity were assessed using a NanoDrop ND-1000 UV spectrophotometer (Thermo Scientific, USA).[20] Aliquots of 5 µg total RNA were used for complementary DNA (cDNA) synthesis by reverse transcription, using the High-Capacity cDNA Reverse Transcription Kit (Thermo Fisher Scientific Inc., Waltham, MA, USA). Quantitative PCR amplification was performed using SYBR Green I Master Mix on a LightCycler® 480 system (Roche, Basel, Switzerland), with gene-specific primers listed in Table 1. Hydroxymethylbilane synthase (HMBS) and hypoxanthine phosphoribosyltransferase 1 (HPRT1) were selected as reference genes, based on minimal variation in Ct values (cycle threshold) across experimental and control conditions. Relative gene expression was calculated using the comparative Ct (ΔΔCt) method, normalised to the geometric mean of the selected housekeeping genes.

Statistical Analysis

All measurements were performed in technical replicates (≥2 per run), and each experimental method was repeated using cells from a minimum of three independent passages ($n \geq 3$). Data are presented as mean ± SD. Statistical analyses were carried out using GraphPad Prism version 8.0 (GraphPad Software Inc., San Diego, CA, USA). The Shapiro–Wilk test was used to assess the normality of data distribution, and the Brown-Forsythe test was employed to evaluate the homogeneity of variances. Where assumptions of normality and equal variance were met, ordinary one-way ANOVA followed by Šidák's multiplicity-adjusted pairwise comparisons was applied. In the presence of heteroscedasticity, we used Welch's ANOVA with Games-Howell post hoc comparisons. For one-versus-control designs, we used Dunnett's test (or Dunnett's T3 under heteroscedasticity). To address multiplicity across assays, we additionally applied the two-stage linear step-up procedure of Benjamini-Krieger-Yekutieli to control the false discovery rate. All tests were two-sided with $\alpha = 0.05$; multiplicity-adjusted P values are reported.

Table 1 Primer Sequences Used for qRT-PCR

Gene	Strand	Sequence 5′ → 3′
Hydroxymethylbilane synthase (*HMBS*)	Forward	GGCAATGCGGCTGCAA
	Reverse	GGGTACCCACGCGAATCAC
Hypoxanthine phosphoribosyltransferase (*HPRT1*)	Forward	TGACACTGGCAAAACAATGCA
	Reverse	GGTCCTTTTCACCAGCAAGCT
Ataxia-telangiectasia mutated (*ATM*)	Forward	GCAGCTGGAAGAAGCACAA
	Reverse	TTTTAGGCTGGGATTGTTCG
ATM and Rad3-related (*ATR*)	Forward	TGTAGAGAGATGGAGACCAACG
	Reverse	GACCAATCGGTTGACTTCTGA
Cyclin-dependent kinase 1 (*CDK1*)	Forward	GGAAACCAGGAAGCCTAGCATC
	Reverse	GGATGATTCAGTGCCATTTTGCC
H2A histone family member X (*γH2AX*)	Forward	ACGAGGAGCTCAACAAGCT
	Reverse	GTGGCGCTGGTCTTCTTG
Poly(ADP-ribose) polymerase (*PARP*)	Forward	GTGTGGGAAGACCAAAGGAA
	Reverse	TTCAAGAGCTCCCATGTTCA

Results

Synthesis and Characterisation of SDS-Based Polyelectrolyte Nanocarriers

The synthesised micelles/polyelectrolyte complexes (Figure 2A), functioning as multicore NCs, exhibited a highly uniform hydrodynamic diameter ranging from ~80 to 100 nm (PDI < 0.3), irrespective of PTX loading or RhoB labelling. These initial NCs presented a positive surface charge (zeta potential: +34 to +37 mV, Figure 2B). Upon subsequent coating with PGA, both empty and PTX-loaded NCs exhibited a negative zeta potential (−32 mV to −49 mV), indicating successful surface modification with the polyanion (Figure 2B). All types of NCs demonstrated excellent colloidal stability in 0.015 M NaCl, maintaining consistent size distribution and zeta potential after storage at ambient temperature (20–22 °C) for over 24 hours (data not shown). Considering the insolubility of PTX in water, its encapsulation efficiency within the NCs was assumed to be 100%. Upon measurement of fluorescence intensity, SDS/PLL/RhoB NCs exhibited approximately 1.5-fold higher signals than SDS/PLL/PGA/RhoB NCs. A corresponding analysis was performed for RhoB-labelled NCs with encapsulated PTX. In this case, no significant difference in fluorescence intensity was observed between the two NC types. These results indicate that PTX incorporation did not interfere with the fluorescence properties of RhoB in the examined SDS-based NCs. A comprehensive summary of all physicochemical parameters for the NCs was presented in Figure 2C.

Cytotoxicity of Multicore SDS-Based Nanocarriers with and without Paclitaxel

In our previous study, we demonstrated that PTX encapsulated in SDS-based multicore NCs retained its cytotoxic properties.[19] Here, we expanded the analysis of the anticancer potential of these nanosystems by evaluating their uptake and the mechanisms of endocytosis involved in the intracellular distribution of SDS/PLL and SDS/PLL/PGA NCs. To enable visual tracking, RhoB was incorporated into the PLL layer of the NCs.

Based on the previous findings, a new batch of NCs was synthesised and used to compare the cytotoxic effects of free PTX with PTX encapsulated in both SDS/PLL and SDS/PLL/PGA NCs. Three concentrations of NCs were tested (12.5 nM, 25 nM, and 50 nM), and intracellular ATP levels were measured after 72 h of incubation using the CellTiter-Glo® assay. Results revealed dose-dependent cytotoxicity for both free PTX and PTX-loaded NCs across all three tested cell lines (Figure 3A–C). Notably, the largest, statistically significant difference versus free PTX at matched dose of PTX encapsulation, was observed in the non-cancerous HMEC-1 cells treated with SDS/PLL/PGA/PTX, including the highest NPs concentration, 50 nM, in comparison with free PTX (Figure 3A, P <0.0001).

To assess whether fluorescent labelling affected cytotoxicity, ATP measurements were conducted in cells treated with SDS/PLL/PTX/RhoB and SDS/PLL/PGA/PTX/RhoB. The presence of RhoB in the PLL layer did not influence the

(A)

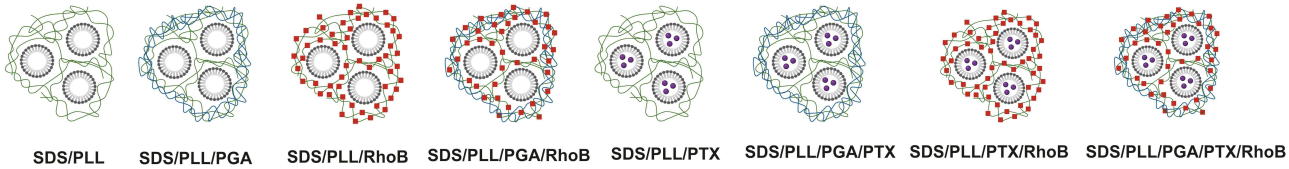

(B)

	SDS/PLL	SDS/PLL/PGA	SDS/PLL/RhoB	SDS/PLL/PGA/RhoB	SDS/PLL/PTX	SDS/PLL/PGA/PTX	SDS/PLL/PTX/RhoB	SDS/PLL/PGA/PTX/RhoB
Size (nm)	91	122	91	122	71	106	91	122
PDI	0.211	0.267	0.226	0.242	0.277	0.281	0.210	0.290
Zeta potential (mV)	+37	-33	+36	-32	+34	-49	+34	-37

(C)

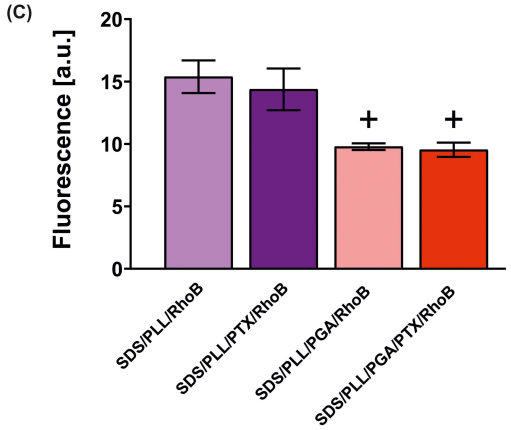

Figure 2 Physicochemical properties of SDS-based NCs. (**A**) Schematic representation of the investigated DDS, illustrating their structure and components. Symbols used in the diagram are green lines – PLL, blue lines – PGA, grey – SDS micelles, red squares – RhoB, purple dots – PTX. (**B**) Hydrodynamic diameter, PDI, and zeta potential of the multicore NCs. (**C**) Fluorescence intensity of SDS/PLL/RhoB and SDS/PLL/PGA/RhoB formulations with or without PTX, respectively. Data are presented as mean ± SD from three independent experiments. +$P < 0.05$ indicates a statistically significant difference between samples in which PGA was added as an additional polyelectrolyte layer.

cytotoxic activity of PTX-loaded NCs in either endothelial or BC cells, except SDS/PLL/PTX/RhoB at the highest PTX concentration (50 nM) in MCF-7 cells (Figure 3B, $P < 0.01$).

PTX Loaded in SDS-Based Nanocarriers Inhibits Global Protein Synthesis

The sensitivity of BC cell lines and human endothelial cells to free PTX and PTX encapsulated in SDS-based NCs was also assessed using a protein synthesis assay. As protein synthesis is essential for cell growth, proliferation, signalling, differentiation, and death, its inhibition reflects changes in cellular physiology.[37] A concentration- and time-dependent decrease in total protein content was observed in MCF-7, MDA-MB-231, and HMEC-1 cells following treatment with increasing concentrations of the tested PTX formulations (Figure 4A–C).

Encapsulation did not systematically enhance PTX-mediated inhibition. Responses with encapsulated PTX generally tracked those of free PTX, with a single condition showing greater inhibition (12.5 nM SDS/PLL/PTX at 72 h in MDA-MB-231; Figure 4C, $P < 0.0001$). In HMEC-1, encapsulation typically attenuated the effect relative to free PTX at matched doses and times (Figure 4A, $P < 0.05$). Differences between the two encapsulated formulations were modest and limited to a few conditions (HMEC-1, 48 h, 50 nM; MDA-MB-231, 48 h, 25 nM; MDA-MB-231, 72 h, 12.5 nM; Figure 4C).

SDS-Based NCs Uptake by Endothelial and Breast Cancer Cells

The uptake of SDS/PLL and SDS/PLL/PGA NCs labelled with RhoB was analysed in MCF-7, MDA-MB-231, and HMEC-1 cells using flow cytometry and fluorescence microscopy. To determine whether active, energy-dependent

https://doi.org/10.2147/NSA.S560473

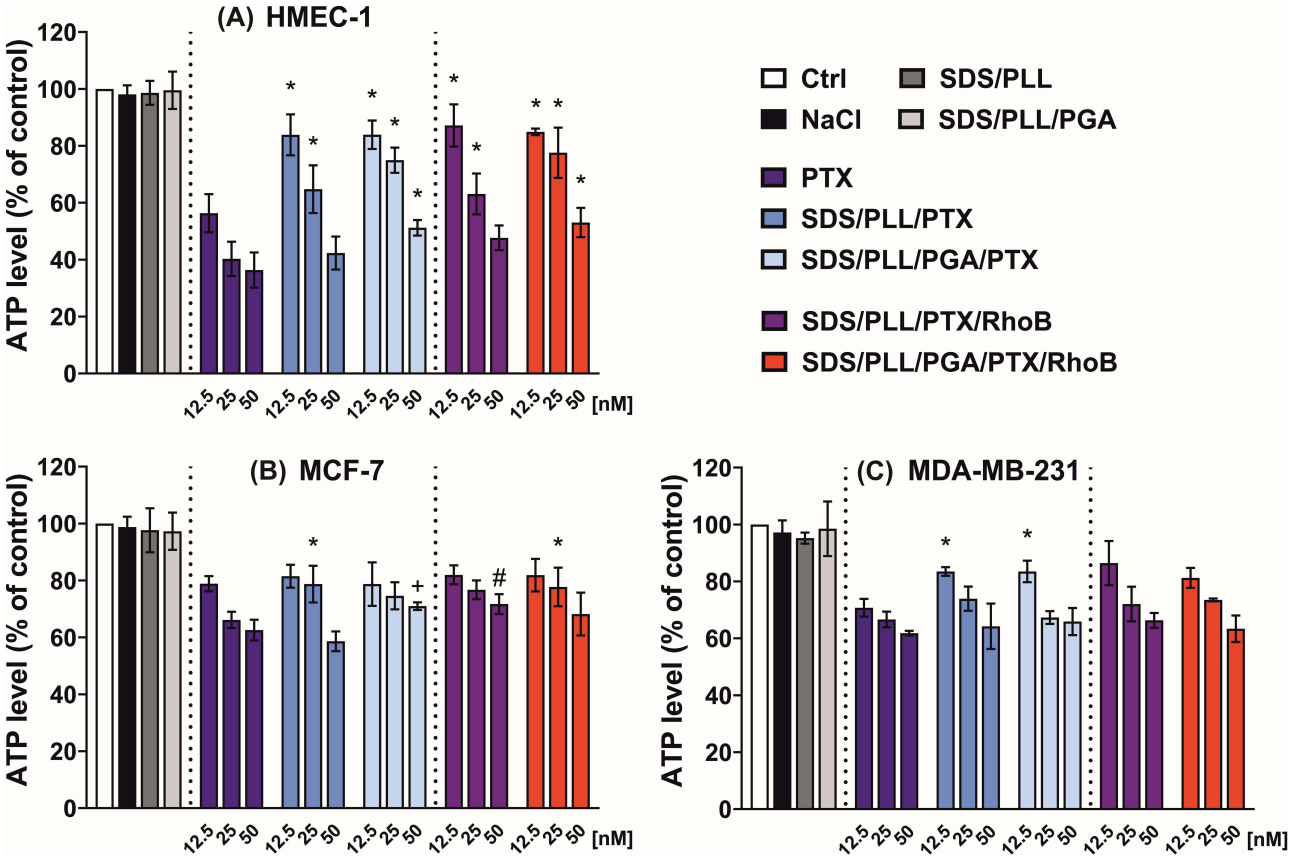

Figure 3 Cytotoxic effects of free PTX and SDS-based NCs. Toxicity of free PTX and various SDS-based NCs formulations: SDS/PLL, SDS/PLL/PGA, SDS/PLL/PTX, and SDS/PLL/PGA/PTX, SDS/PLL/PTX/RhoB, SDS/PLL/PGA/PTX/RhoB, was evaluated in HMEC-1 (**A**), MCF-7 (**B**), and MDA-MB-231 (**C**) cells. Cell viability was evaluated based on ATP content after 72 hours of incubation with the tested compounds. Data are presented as mean ± SD from four independent experiments. **P* <0.05 indicates statistical significance of differences between cells treated with PTX and SDS/PLL/PTX or SDS/PLL/PGA/PTX. #*P* <0.05 indicates significance of differences between NCs loaded with PTX and NCs loaded with PTX additionally stained with RhoB.

transport mechanisms mediated the cellular uptake of SDS-based NCs, cells were incubated with RhoB-labelled NCs (1×10^7 NCs/mL) at 37 °C for up to 2 hours. In parallel, control samples were incubated at 4 °C to suppress active transport. Next, the cells were washed with PBS and analysed by flow cytometry. In the control samples incubated at 4 °C, the intracellular transport of NCs was effectively suppressed, as demonstrated in Figure 5A, indicating that cellular uptake of SDS-based NCs is mediated by energy-dependent, endocytic processes.

For cells incubated at 37 °C, the intensity of fluorescence depended on the NC type. It was approximately 30-fold higher in cells treated with SDS/PLL/RhoB compared to those treated with SDS/PLL/PGA/RhoB (see Y-axis: scale up to 60,000 for PLL-coated vs 2000 for PLL/PGA-coated NCs in Figure 5A and B). This observation, corroborated by fluorescence microscopy performed in parallel, suggests that the additional polyelectrolyte layer composed of PGA attenuated the signal emitted by the RhoB fluorophore. Representative fluorescence images of HMEC-1, MCF-7, and MDA-MB-231 cells treated with SDS-based NCs are shown in Figure 5C and D. When intracellular accumulation of the same NC type was compared across the three cell lines after 2 hours of incubation, no statistically significant differences were observed (Figure 5A and B). However, time-course analysis over 4 hours revealed distinct dynamics of NCs uptake (Supplementary Figure 1 and Supplementary Table 2). SDS/PLL/PGA NCs showed approximately two-fold lower accumulation in HMEC-1 cells compared to MCF-7 and MDA-MB-231 cells.

Given that active transport mechanisms mediate the intracellular uptake of SDS-based NCs, we next investigated whether the concentration of FBS influences their endocytosis. A key determinant of nanomaterial-cell interactions is the composition of the protein corona that forms on the surface of NPs in biological fluids like serum.[38] To assess the impact of serum concentration, the uptake of RhoB-labelled NCs was evaluated in the presence of either 1% or 10% FBS. As

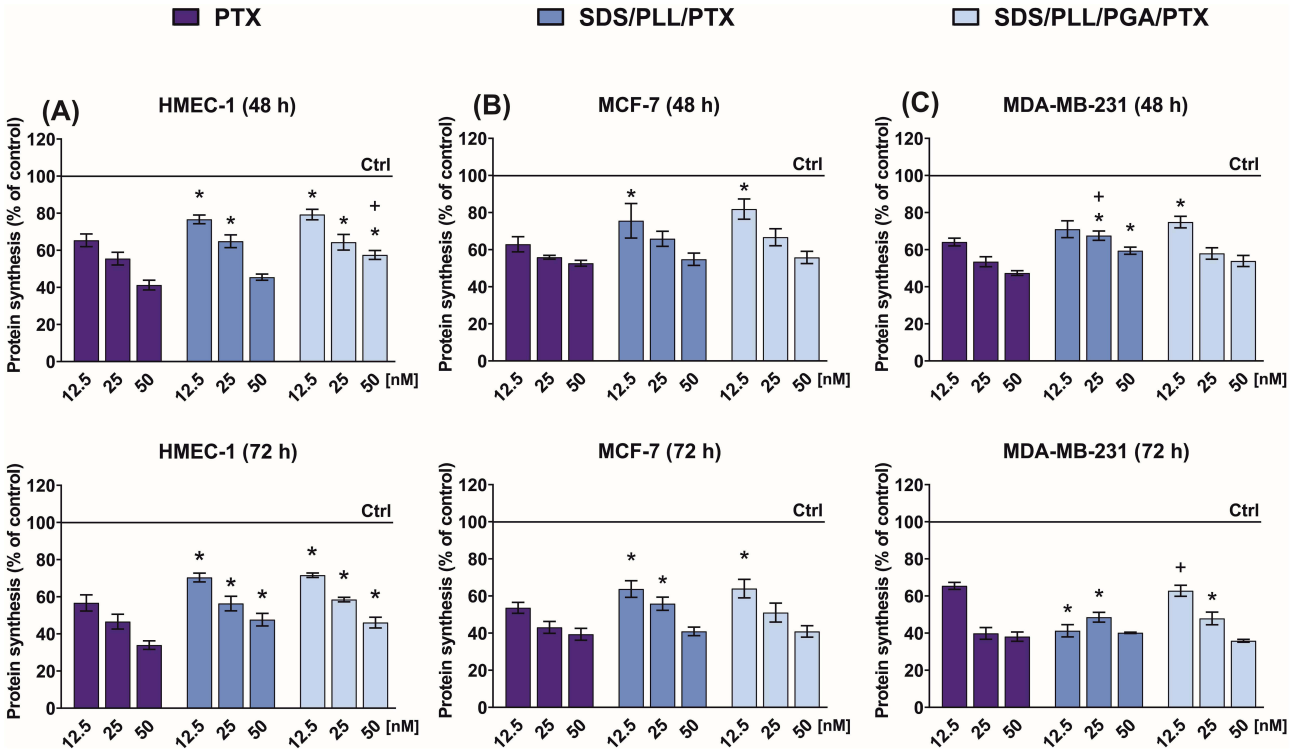

Figure 4 Inhibition of protein synthesis in non-cancerous endothelial cells and BC cell lines. Protein synthesis was determined in HMEC-1 (**A**), MCF-7 (**B**), and MDA-MB-231 (**C**) cell lines following exposure to PTX, SDS/PLL/PTX, or SDS/PLL/PGA/PTX at concentrations of 12.5, 25, and 50 nM for 48 and 72 hours. Data are presented as mean ± SD from four independent experiments. **P* <0.05 indicates statistical significance of differences between cells treated with PTX and SDS/PLL/PTX or SDS/PLL/PGA/PTX. +*P* <0.05 indicates significance of differences between SDS/PLL/PTX and SDS/PLL/PGA/PTX.

shown in Figure 5A, enhanced uptake of both SDS/PLL/RhoB and SDS/PLL/PGA/RhoB was observed when cells were cultured in medium supplemented with 1% FBS ($P < 0.01$). Notably, the highest level of particles was detected in HMEC-1 endothelial cells, with fluorescence intensities reaching 49,000 a.u. for SDS/PLL/RhoB and 1700 a.u. for SDS/PLL/PGA/RhoB.

As shown above, the cellular uptake of SDS-based NCs is mediated by temperature-dependent, endocytic processes. Thus, the uptake of SDS/PLL/RhoB or SDS/PLL/PGA/RhoB NCs was measured using a panel of clathrin-dependent and -independent inhibitors (Supplementary Table 1) at appropriate concentrations to block endocytic pathways and assess mechanisms of NCs internalization. Strikingly, treatment with these inhibitors of cellular transport mechanisms allowed us to obtain consistent data for both examined forms of NCs across all tested cell types. Dynasore is known to inhibit dynamin, a key protein involved in clathrin-mediated vesicle formation (Supplementary Table 1), fast endophilin-mediated endocytosis (FEME), Ras homolog family member A (RhoA)-dependent uptake, and caveolae-mediated uptake. When MCF-7, MDA-MB-231, and HMEC-1 cell lines were incubated with dynasore, the uptake of fluorescent SDS/PLL NCs was significantly reduced ($P < 0.0001$). In contrast, in all examined cells treated with SDS/PLL/PGA/RhoB in the presence of dynasore, particle uptake remained unchanged, indicating that dynamin activity is not essential for the endocytosis of SDS/PLL/PGA NCs (Figure 6A–C).

The intracellular transport of both SDS/PLL and SDS/PLL/PGA particles was also not mediated by caveolae-dependent pathways. Supporting this, we observed no effect of genistein, which inhibits tyrosine kinases and can block caveolae-mediated uptake (Figure 6A–C). Furthermore, since caveolae are 50–80 nm in diameter,[39] these membrane structures are unlikely to be involved in the internalization of much larger NCs such as NCS, SDS/PLL (71–91 nm), or SDS/PLL/PGA (106–122 nm).

The extraction of cholesterol (necessary for caveolae formation) by methyl-β-cyclodextrin significantly diminished the uptake of both examined types of SDS-based NCs (Figure 6A–C, $P < 0.01$). However, cholesterol is a crucial component of mammalian cellular membranes, being essential not only for caveolae formation but also for dynamin-

https://doi.org/10.2147/NSA.S560473

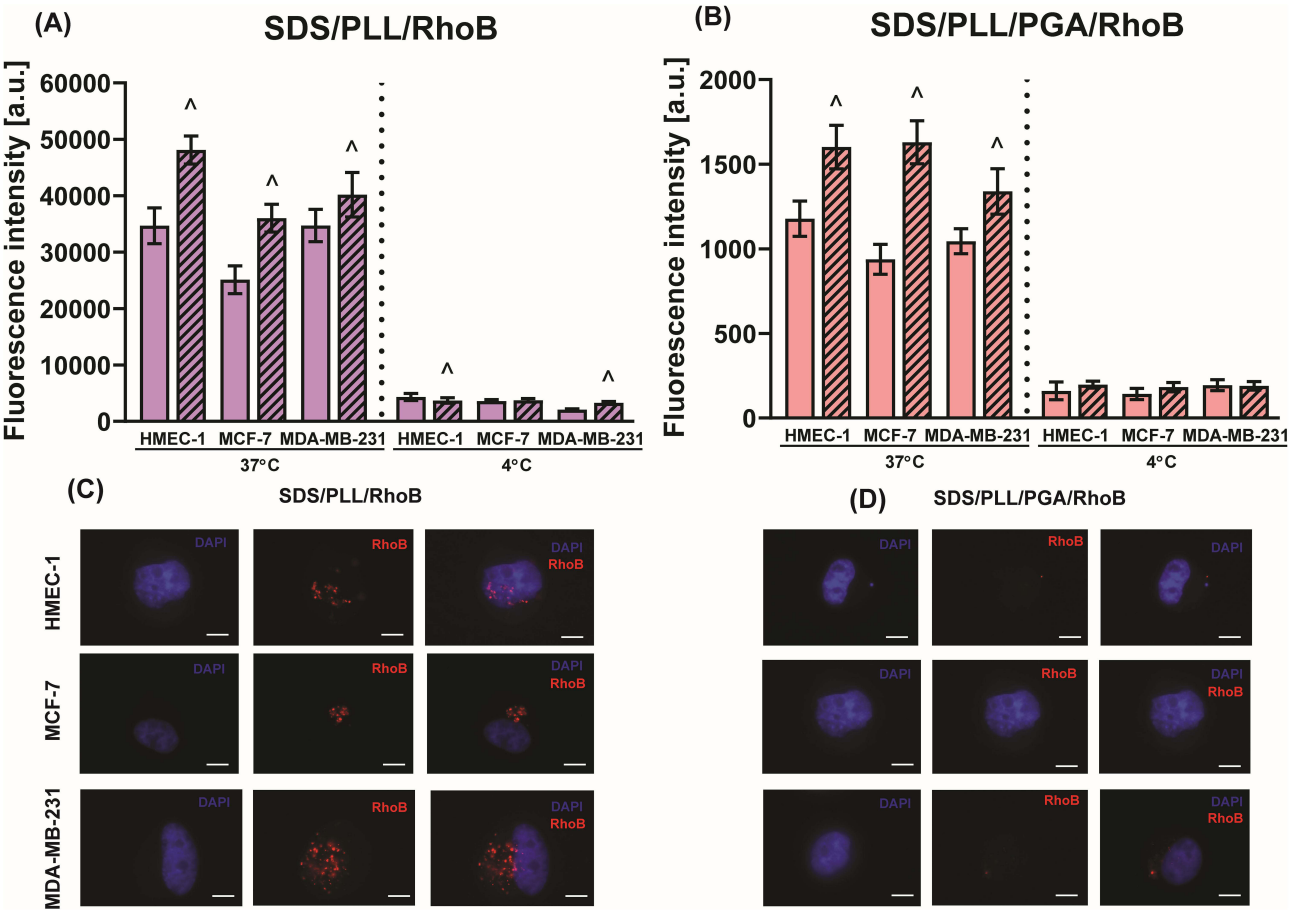

Figure 5 Intracellular transport of SDS-Based NCs labelled with RhoB in HMEC-1, MCF-7, and MDA-MB-231 cells. Uptake of SDS/PLL/RhoB (**A**) (lavender color) and SDS/PLL/PGA/RhoB NCs (**B**) (raspberry color) after 2 hours of incubation at either 37 °C or 4 °C with 1×10^7 NCs/mL NCs in cell culture medium supplemented with 10% (plain-pattern bars) or 1% (stripe-pattern bars) FBS. Data are presented as mean ± SD, n = 4. ^*P* <0.05 indicates significant differences between conditions with 1% and 10% FBS. Representative fluorescence microscopy images showing the uptake of RhoB-labelled capsules: SDS/PLL (**C**) or SDS/PL/PGA NCs (**D**) by HMEC-1, MCF-7, and MDA-MB-231 cells. Immediately following flow cytometry analysis, cells were collected and fixed with 4% paraformaldehyde. Nuclei were stained with DAPI (5 μg/mL), and fluorescence imaging was performed using a Nikon Eclipse TE2000-U microscope equipped with a digital color camera and a 10× Plan Fluor objective. Scale bar denotes 10 μm.

dependent endocytosis and macropinocytosis. Thus, cholesterol depletion may inhibit the formation of macropinosomes. The involvement of macropinocytosis in the uptake of both SDS/PLL and SDS/PLL/PGA NCs was confirmed by the noticeable inhibitory effect of 5-(N-ethyl-N-isopropyl)amiloride (EIPA), a drug that blocks Na+/H+ exchange[40,41] (Figure 6A–C, $P < 0.01$). Interestingly, treatment with latrunculin B, a compound known to disrupt actin filament formation during macropinocytosis,[42] selectively reduced the uptake of SDS/PLL NCs ($P < 0.001$), but had no significant effect on SDS/PLL/PGA NCs (Figure 6A–C). Similar inhibitory effects ($P < 0.01$) were observed upon application of wortmannin, a phosphoinositide 3-kinase (PI3K) inhibitor, which impairs macropinosome formation and also affects cell division control protein 42 homolog (Cdc42)-dependent pathways,[43] including GRAF1-mediated CLIC (clathrin-independent carriers) and GEEC (glycosylphosphatidylinositol-anchored protein-enriched endosomal compartment) routes.[44]

To further investigate the involvement of Cdc42, cells were preincubated with ML141, a selective Cdc42 inhibitor. However, this approach did not permit discrimination between the aforementioned endocytic pathways, as all tested cell lines showed reduced uptake of SDS/PLL NCs (Figure 6A–C, $P < 0.0001$). Taken together, these findings demonstrate that exposure of cells to SDS-based NCs engages multiple endocytic pathways. The SDS/PLL NCs are internalized predominantly via the dynamin-dependent and macropinocytosis mechanisms, whereas the uptake of SDS/PLL/PGA NCs is mainly dependent on macropinocytic processes.

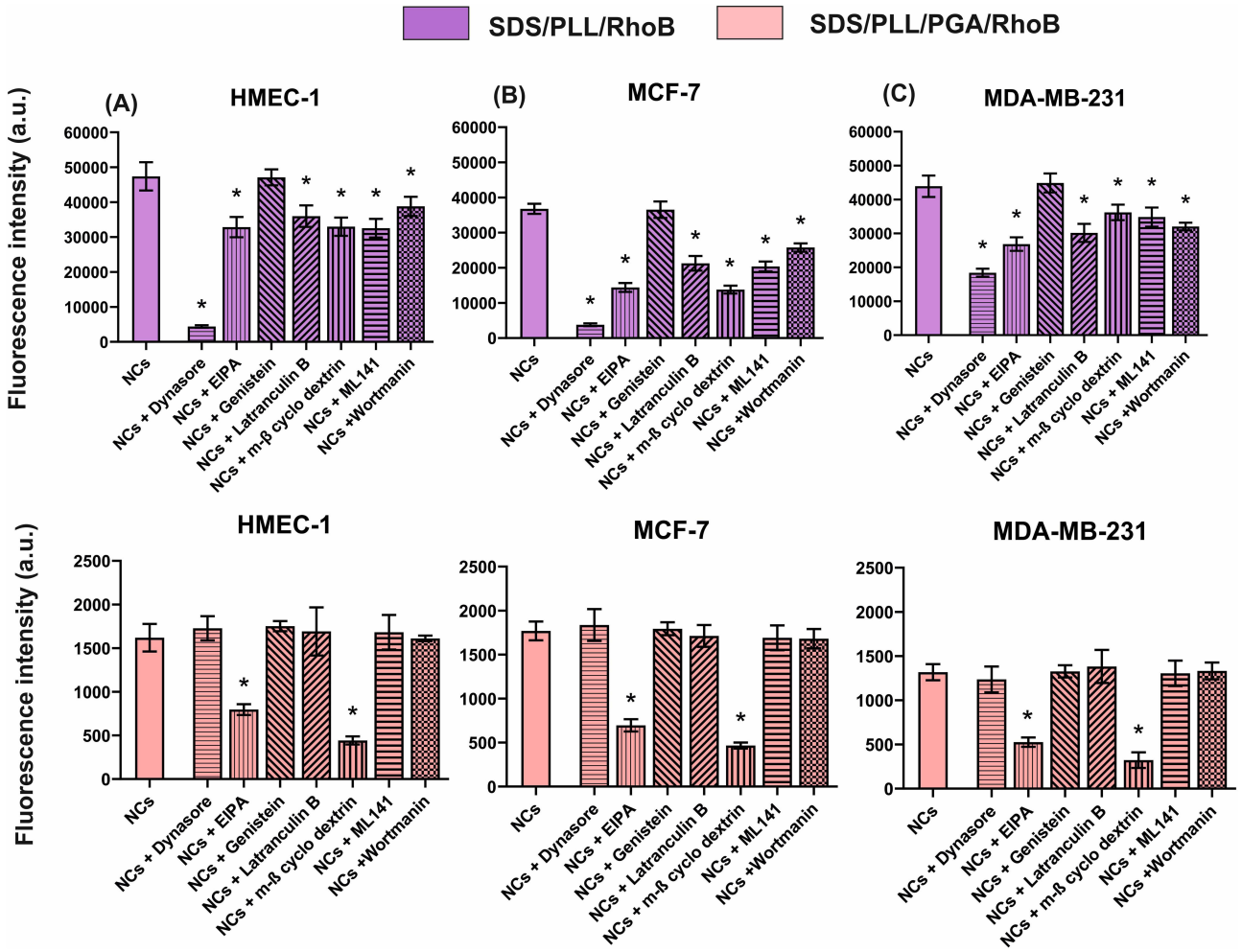

Figure 6 Endocytic mechanisms involved in the uptake of SDS-based NCs. (**A** and **C**) Uptake of RhoB-labelled SDS-based NCs by endothelial HMEC-1 cells (**A**) and BC cell lines (MCF-7 (**B**), MDA-MB-231 (**C**)). Cells were pretreated with specific endocytosis inhibitors for 30 minutes at 37 °C in growth medium supplemented with 1% FBS. Subsequently, cells were incubated with 0.5 mg/mL SDS-based NCs in the same medium for 2 hours at 37 °C. Fluorescence intensity was quantified by flow cytometry. Data are presented as mean ± SD, n = 3. *P <0.05 indicates significant differences compared to untreated control cells (without inhibitors).

DNA Lesions Induced by SDS-Based NCs Indicate the Genotoxicity of PTX Encapsulated in Nanoparticles

A decrease in ATP levels demonstrated in cell cultures (Figure 3A–C) is often considered a hallmark of global cellular toxicity of analysed NPs, particularly when associated with DNA damage.[45] Therefore, in this study, we evaluated whether the investigated SDS-based NCs induced DNA single- and double-strand breaks as well as alkali-labile sites, based on the percentage of degradable DNA detected by the comet assay.[46]

Following our above-described cytotoxicity studies,[19] the extent of DNA damage induced by PTX released from SDS/PLL/PTX or SDS/PLL/PGA/PTX was evaluated after 48 and 72 hours of incubation of cells with NCs. As expected, the longer the exposure to SDS-based particles loaded with PTX, the greater the percentage of degraded DNA, as shown in the comet tail analysis (Figure 7A–C). Interestingly, after 72 hours of treatment, no changes in DNA fragmentation were observed in either BC cell line treated with free PTX compared to SDS/PLL/PTX at concentrations of 25 or 50 nM (Figure 7B and C). In contrast, a significant decrease in comet tail DNA percentage was noted in HMEC-1 endothelial cells treated with SDS/PLL/PTX or SDS/PLL/PGA/PTX by 72 hours (Figure 7A, P <0.05), compared to cells exposed to free PTX, suggesting greater sensitivity of endothelial cells to the free form of the drug. Statistically significant differences between the two encapsulated PTX formulations were observed in MCF-7 and MDA-MB-231 cells (Figure 7B and C, P <0.05).

https://doi.org/10.2147/NSA.S560473

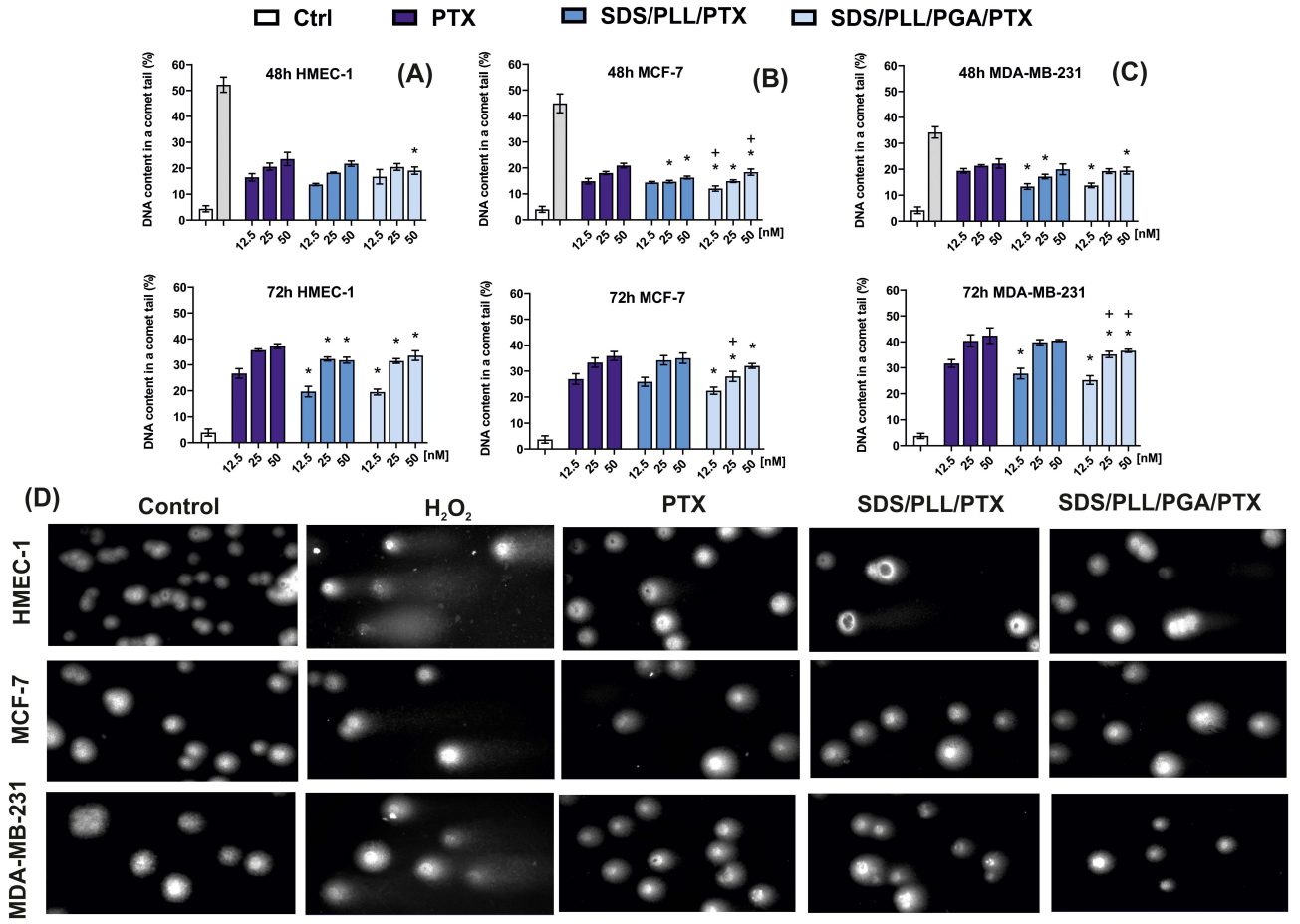

Figure 7 Genotoxicity of SDS/PLL/PTX and SDS/PLL/PGA/PTX in human BC cells (MCF-7, MDA-MB-231) and in non-cancerous HMEC-1 cells. DNA damages were determined in HMEC-1 (**A**), MCF-7 (**B**), and MDA-MB-231 (**C**) cells, using the alkaline comet assay (pH > 13), which quantifies the percentage of DNA in the comet tail. Cells were exposed to various PTX formulations (12.5, 25, and 50 nM) for 48 and 72 hours. **P* <0.05 indicates significant differences between cells treated with free PTX and SDS/PLL/PTX or SDS/PLL/PGA/PTX. +*P* <0.05 indicates significant differences between SDS/PLL/PTX and SDS/PLL/PGA/PTX treatments. (**D**) Representative fluorescence microscopy images of comets from non-cancerous and malignant cells treated with free PTX or PTX-loaded SDS-based NCs. Images were acquired using an inverted fluorescence microscope (Nikon, Tokyo, Japan) at 200× magnification.

Consistent with the quantified DNA damage, representative images of comets were presented for control cells and those treated with the tested compounds. As shown in Figure 7D, the comets from control cells displayed a nearly symmetrical morphology with no visible tails. In contrast, cells treated with free PTX or PTX encapsulated in SDS-based NCs exhibited pronounced comet tails. Interestingly, the number of comets analysed per slide was markedly lower in control samples than in those treated with the tested PTX formulations. Moreover, comet assay images following treatment with encapsulated PTX clearly showed nuclei surrounded by extensive DNA fragmentation (Figure 7D).

Since DNA damage detected by the comet assay may include double-strand breaks (DSBs),[46] we next evaluated changes in the phosphorylation of γH2AX, a DSB marker. As shown in Figure 8A, free PTX induced a fivefold increase in γH2AX phosphorylation level in HMEC-1 cells after 72 hours of incubation, whereas PTX incorporated into NCs resulted in a lower percentage of DSBs compared to the drug alone (P <0.0001). In MCF-7 and MDA-MB-231 cells, SDS/PLL/PTX elicited γH2AX phosphorylation comparable to that induced by free PTX at 72 h (Figure 8B and C). The significantly lower γH2AX phosphorylation compared to PTX and SDS/PLL/PTX was observed in MCF-7 after 48 h of treatment with SDS/PLL/PGA/PTX (Figure 8B and C, P <0.01).

Interestingly, in HMEC-1 cells, H2AX mRNA levels were significantly higher with both PTX-loaded capsules (SDS/PLL/PTX and SDS/PLL/PGA/PTX) at 50 nM than with free PTX (Figure 8D, P <0.0001). Furthermore, neither SDS/

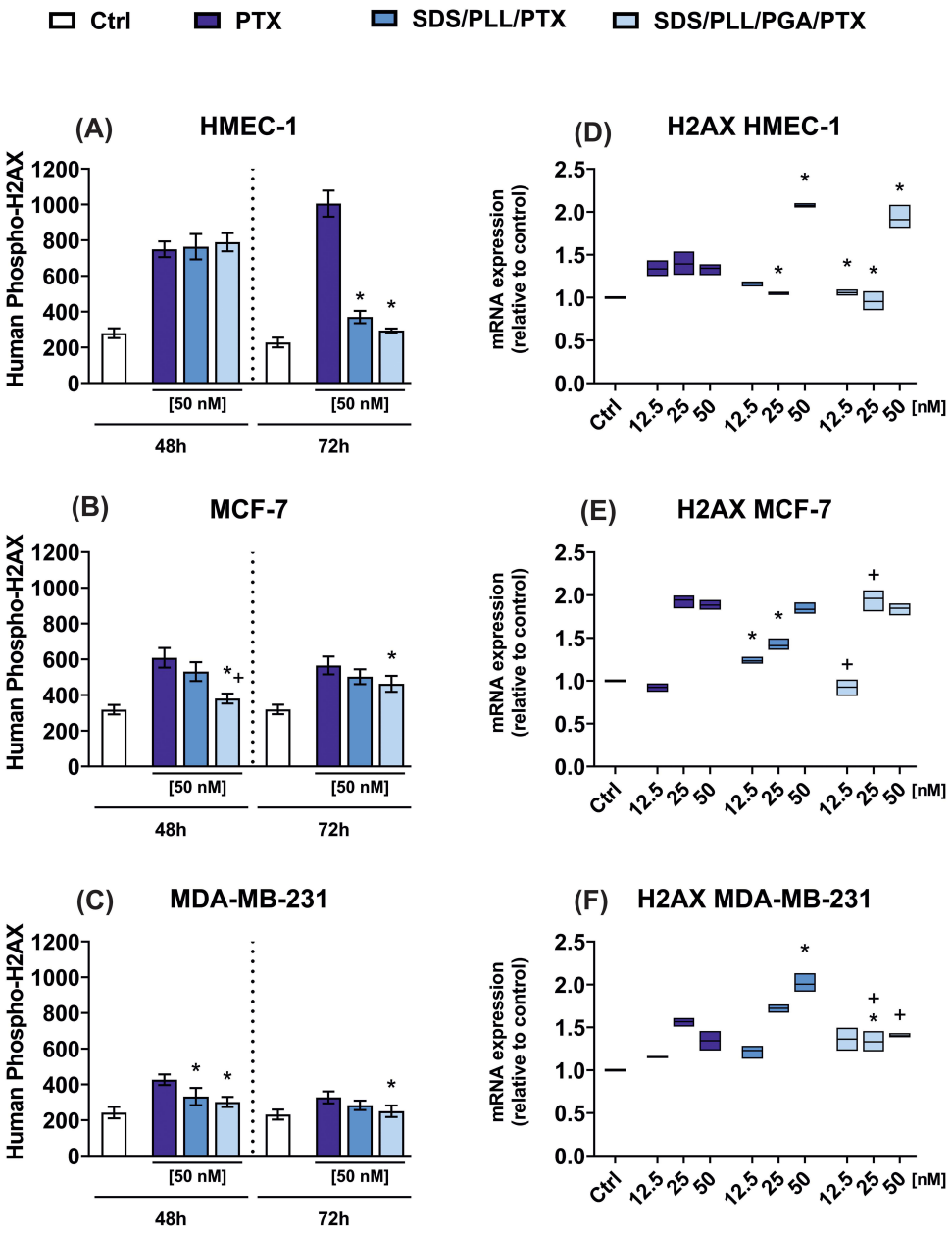

Figure 8 PTX encapsulated in SDS/PLL or SDS/PLL/PGA NCs induces histone γH2AX modifications in human BC and endothelial cells. (**A** - **C**) Phosphorylation of histone γH2AX was assessed in HMEC-1 (**A**), MCF-7 (**B**), and MDA-MB-231 (**C**) cells following treatment with 50 nM of free PTX, SDS/PLL/PTX, or SDS/PLL/PGA/PTX for 48 or 72 hours. All values were normalized to total cellular protein content, as determined by the bicinchoninic acid (BCA) assay. Data are presented as mean ± SD, n = 4.* *P* <0.05 indicates statistically significant differences between cells treated with free PTX and those treated with PTX-loaded NCs. +*P* <0.05 indicates significant differences in γH2AX phosphorylation levels between cells treated with SDS/PLL/PTX and SDS/PLL/PGA/PTX. (**D** - **F**) mRNA expression levels of the γH2AX gene were measured in HMEC-1 (**D**), MCF-7 (**E**), and MDA-MB-231 cells (**F**) after 48-hour exposure to 12.5, 25, or 50 nM of free PTX, SDS/PLL/PTX, or SDS/PLL/PGA/PTX. Data are presented as mean ± SD, n = 3. **P* <0.05 indicates statistically significant differences in γH2AX mRNA levels in cells treated with PTX-loaded NCs compared to those incubated with PTX alone. +*P* <0.05 indicates significant differences in γH2AX mRNA levels between SDS/PLL/PTX and SDS/PLL/PGA/PTX treatments.

PLL/PTX nor SDS/PLL/PGA/PTX treatment in MCF-7 cells resulted in an increase in H2AX transcription compared to PTX alone (Figure 8E, $P < 0.005$). In MDA-MB-231 cell line, SDS/PLL/PGA/PTX at 25 and 50 nM led to lower H2AX mRNA levels compared to SDS/PLL/PTX (Figure 8F, $P < 0.001$).

https://doi.org/10.2147/NSA.S560473

Changes in Cell Cycle Distribution and PARP Activity are Associated with Apoptosis Induction by PTX Encapsulated in SDS-Based NCs

Given that PTX is a cytostatic anticancer agent that inhibits cancer cell proliferation, we next investigated whether DNA lesions induced by SDS/PLL/PTX or SDS/PLL/PGA/PTX result from alterations in the expression of ATM, ATR, and CDK1 genes, widely recognized as sentinels of genome stability.[47] Treatment with SDS/PLL/PGA/PTX increased ATM mRNA expression in MDA-MB-231 cells compared with free PTX (Figure 9A, P <0.05). In contrast, ATR mRNA levels were generally lower after exposure to both PTX-loaded capsules (SDS/PLL/PTX and SDS/PLL/PGA/PTX) than with free PTX P, except in MCF-7 cells treated with 50 nM SDS/PLL/PTX, where ATR mRNA was increased (Figure 9B, P <0.0001). Additionally, in MCF-7 cells, CDK1 expression was increased twofold following treatment with 12.5 and 25 nM SDS/PLL/PTX or SDS/PLL/PGA/PTX, compared to cells treated with PTX alone (Figure 9C, P <0.05).

Following the observed changes in mRNA levels of ATM, ATR, and CDK1 kinases, we examined whether cell cycle distribution is affected by SDS/PLL/PTX or SDS/PLL/PGA/PTX (Figure 10A). As shown in Figure 10B and C, free PTX induced a more pronounced arrest of G2/M phase compared to PTX encapsulated in SDS-based NCs in HMEC-1 and MCF-7 cells (P <0.001). In contrast, in MDA-MB-231, this difference was evident only at 50 nM (Figure 10D, P <0.05). Furthermore, in HMEC-1 and MCF-7 cells, SDS/PLL/PTX was associated with a higher G2/M-phase fraction

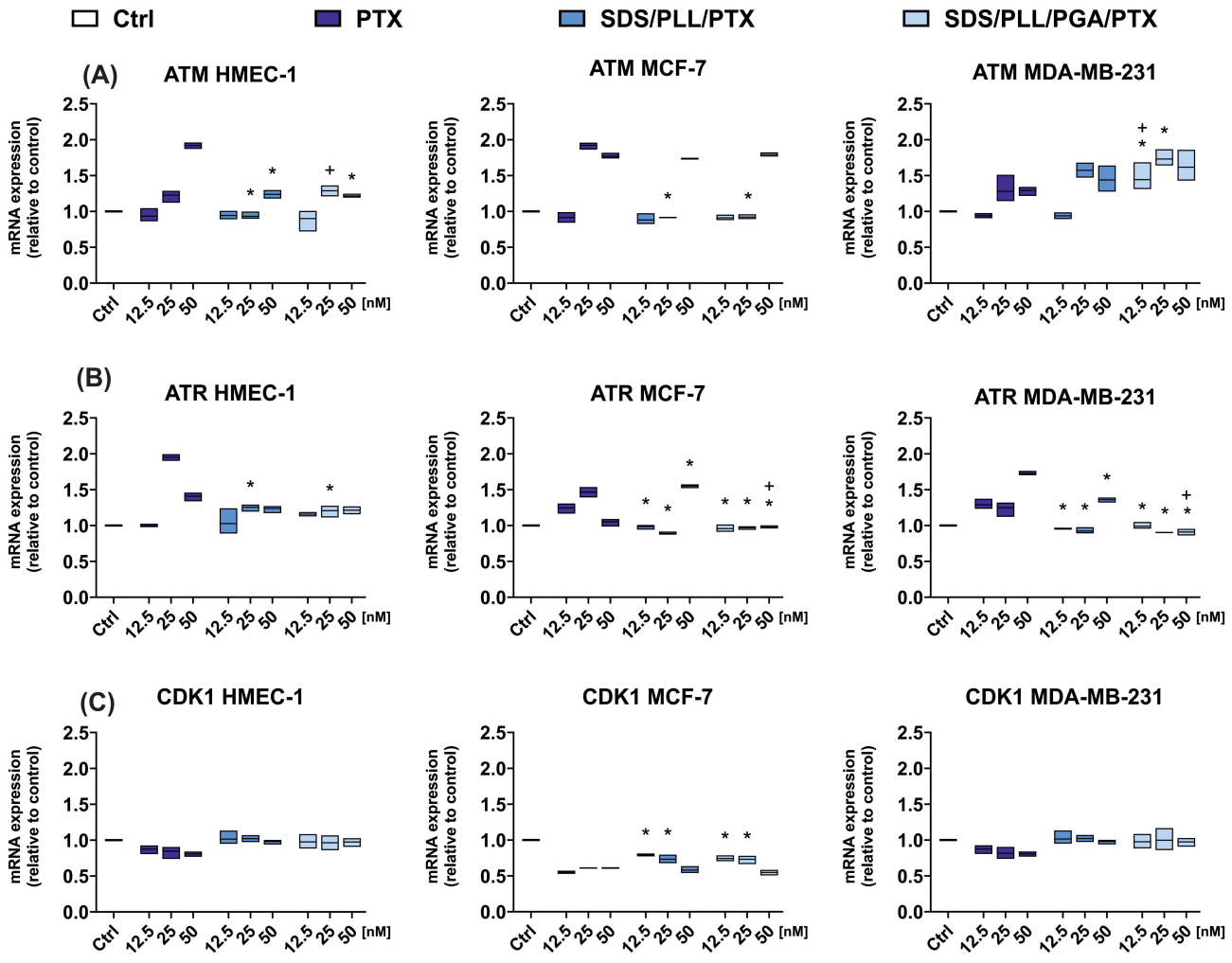

Figure 9 Expression levels of ATR (**A**), ATM (**B**), and CDK1 (**C**) mRNA in HMEC-1, MCF-7, and MDA-MB-231 cells. Cells were exposed to 12.5 nM, 25 nM, and 50 nM of free PTX, SDS/PLL/PTX, or SDS/PLL/PGA/PTX for 48 hours. Gene expression levels were assessed by quantifying ΔCt values, which were then converted into the number of mRNA copies per housekeeping gene index and normalized to the expression levels in control cells (set as 1). Results are presented as mean ± SD, n = 3. *P <0.05 indicates statistically significant differences in mRNA levels between cells treated with free PTX and those treated with PTX encapsulated in SDS-based NCs. +P <0.05 denotes significant differences between cells treated with SDS/PLL/PTX and SDS/PLL/PGA/PTX.

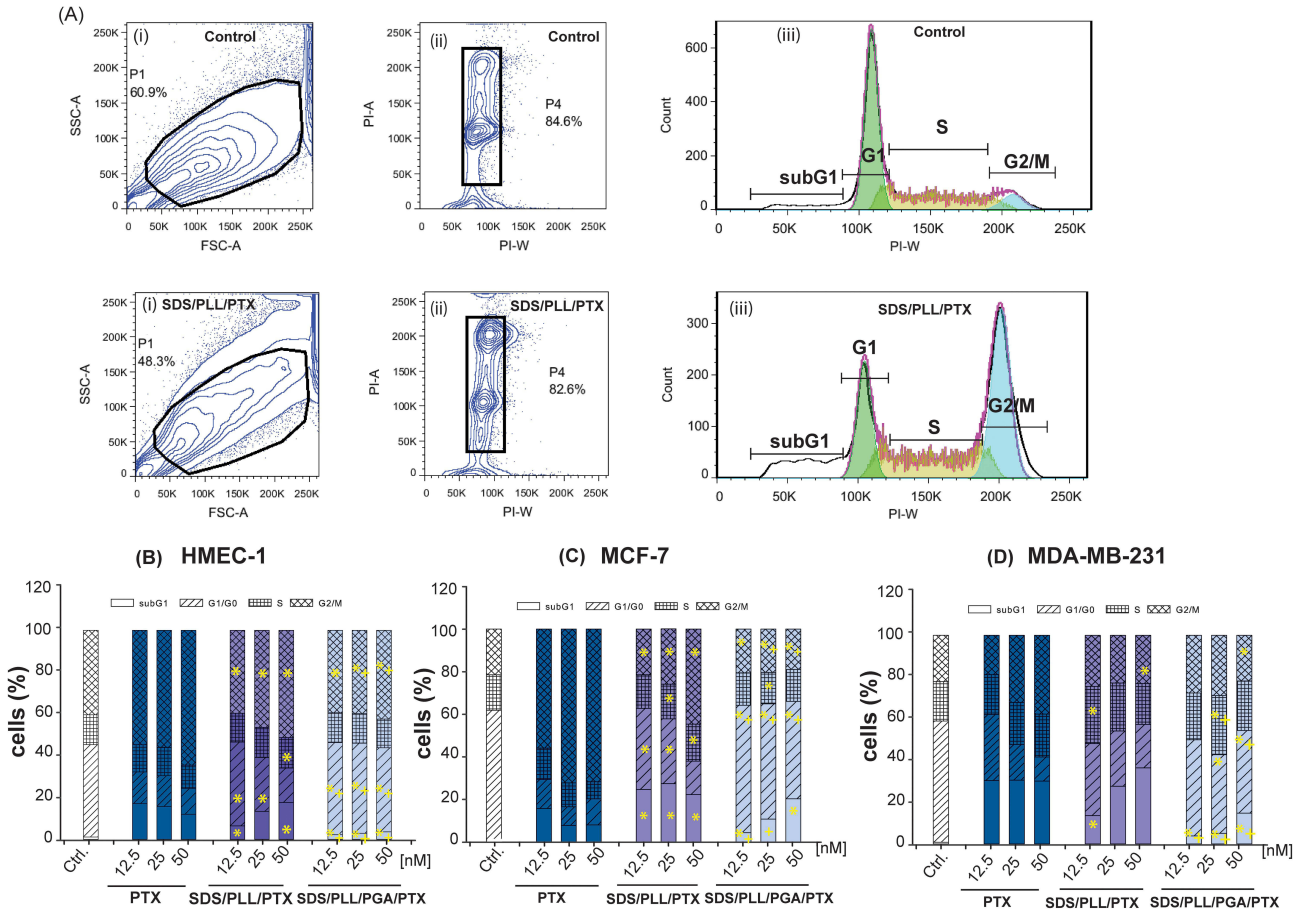

Figure 10 Assessment of the cell cycle distribution (**A**) Representative flow cytometry analysis of MCF-7 cells exposed to vehicle control (PBS) or SDS/PLL/PTX. Cells were fixed and stained with PI. Gating strategy: First, doublets and cell debris were excluded in the FSC-A vs SSC-A (i) analysis. Next, the distribution of cells across different cell cycle phases was determined based on DNA content (ii) in fluorescence signal area vs fluorescence signal width (PI-A vs PI-W) analysis. Finally PI-A histograms of the cells gated in (i) and (ii), exposed to various forms of PTX, were calculated (iii); (**B** and **D**) Distribution of cell cycle phases in HMEC-1 (**B**), MCF-7 (**C**), and MDA-MB-231 (**D**) cells following 48 hours of incubation with 12.5 nM, 25 nM, or 50 nM of free PTX, SDS/PLL/PTX, or SDS/PLL/PGA/PTX. Values represent the mean ± SD from four independent experiments. *P <0.05 indicates statistically significant differences between cells treated with free PTX and those treated with PTX-loaded SDS-based NCs. +P <0.05 indicates significant differences between cells treated with SDS/PLL/PTX and SDS/PLL/PGA/PTX.

than SDS/PLL/PGA/PTX at 25 and 50 nM (Figure 10B and C, P <0.01). Notably, the most prominent difference was observed in MCF-7 cells, where treatment with free PTX (50 nM) resulted in a 3.8-fold higher proportion of G2/M cells compared to cells treated with SDS/PLL/PGA/PTX (Figure 10C).

Moreover, in both HMEC-1 and MCF-7 cells, SDS/PLL/PGA/PTX consistently increased the G1/G0 fraction more than either SDS/PLL/PTX or free PTX across all applied concentrations (Figure 10B and C, P <0.01). In contrast, this phenomenon was observed in MDA-MB-231 cells only at 50 nM of SDS/PLL/PGA/PTX (Figure 10D, P <0.01).

In parallel with the cell cycle analyses, we assessed the proportion of cells in the sub-G1 phase, a marker of DNA fragmentation typically associated with apoptosis. Notably, treatment of MCF-7 cells with SDS/PLL/PTX resulted in an increased level of sub-G1 cell population compared to free PTX, in all applied concentrations (Figure 10C, P <0.0001). Furthermore, both HMEC-1 and MDA-MB-231 cell lines exhibited a significant reduction in the sub-G1 fraction when treated with SDS/PLL/PGA/PTX, compared to cells exposed to free PTX or SDS/PLL/PTX (Figure 10A and C, P <0.05).

Given PARP's central role in DNA damage responses and its caspase-dependent inactivation during apoptosis, we next assessed PARP level following exposure to free PTX versus SDS-based PTX nanocarriers (Figure 11A–C). The differences between free PTX and SDS/PLL/PTX or SDS/PLL/PGA/PTX were most pronounced in BC cells, where PTX increased PARP level significantly higher than encapsulated forms of the drug (Figure 11B and C, P <0.05). The

https://doi.org/10.2147/NSA.S560473

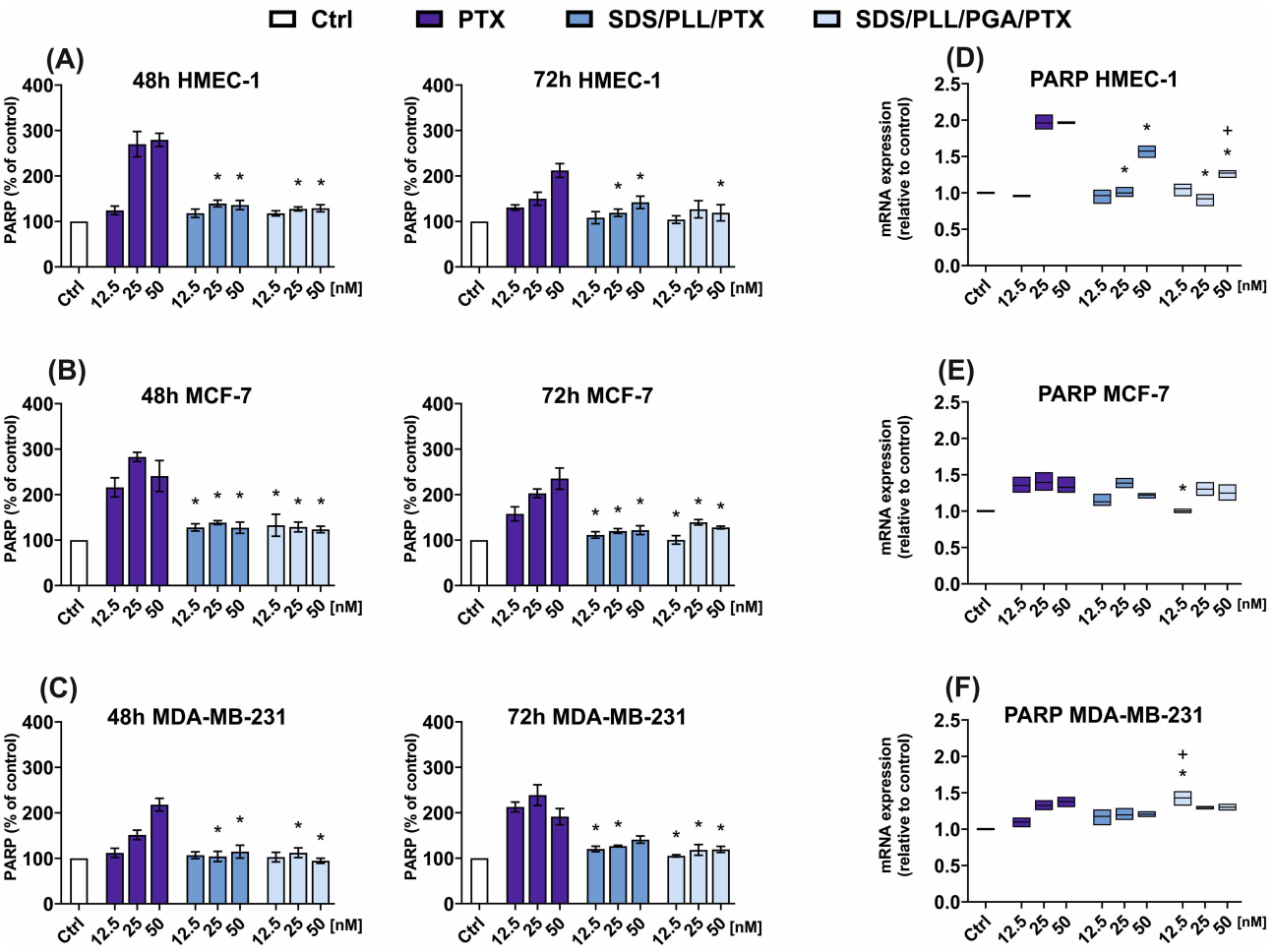

Figure 11 Alterations in PARP activity and transcription in BC and non-cancerous endothelial cells treated with SDS-Based NCs. (**A** - **C**) Effects of free PTX, SDS/PLL/PTX, and SDS/PLL/PGA/PTX on PARP activity (expressed as a percentage of control) in HMEC-1 (**A**), MCF-7 (**B**), and MDA-MB-231 (**C**) cells. Cells were treated with 12.5 nM, 25 nM, or 50 nM of the respective formulations for 48 and 72 hours. All values were normalised to untreated control cells (set as 100%). Data are presented as mean ± SD from four independent experiments. **P* <0.05 indicates statistically significant differences between cells treated with free PTX and those treated with PTX-loaded NCs. (**D** - **F**) PARP mRNA expression levels (relative to HPRT1) in HMEC-1 (**D**), MCF-7 (**E**), and MDA-MB-231 (**F**) cells following 48-hour exposure to the tested PTX formulations (12.5 nM, 25 nM, and 50 nM). **P* <0.05 indicates statistically significant differences in transcription levels between cells treated with NCs-encapsulated PTX and those treated with free PTX. +*P* <0.05 indicates significant differences between cells treated with SDS/PLL/PTX and SDS/PLL/PGA/PTX.

functional involvement of PARP in both DNA repair and apoptosis was further supported by the analysis of PARP mRNA expression. The clearest difference was observed in HMEC-1, where both SDS/PLL/PTX and SDS/PLL/PGA/PTX reduced PARP transcript levels relative to free PTX at 25 and 50 nM (Figure 11D, P <0.0001). In contrast, in both BC cell lines, only minor alterations were observed between the PTX-loaded nanocarriers and the free drug (Figure 11E and F).

Discussion

In this study, we demonstrate that differential cellular effects of PTX encapsulated in SDS-based polyelectrolyte nanocarriers are linked to their uptake mechanisms, consistent across endothelial and breast cancer models, and contextualized by serum-dependent modulation of internalization. Labeling the NCs with RhoB enabled the visualization of capsules within cells without affecting the viability of either malignant or non-cancerous cell lines. Uptake of both SDS/PLL and SDS/PLL/PGA NCs was shown to be an active, energy-dependent process, and higher concentrations of serum in the culture medium reduced the extent of NCs internalization. The presence of an additional polyelectrolyte layer (PGA) over PLL-RhoB resulted in a markedly attenuated fluorescence signal emitted by SDS/PLL/PGA/Rho NCs. Surprisingly, differences in uptake between SDS-based NCs were up to 30-fold across endothelial, epithelial, and

mesenchymal-like cell types. These findings suggest that the physicochemical properties of the NCs, such as surface charge, are critical determinants of their cellular internalization. Finally, we showed that treatment with PTX delivered via SDS-based NCs led to a concentration-dependent reduction in intracellular ATP levels and inhibition of protein synthesis (Figures 3 and 4). The cytotoxic and genotoxic effects of PTX administered through SDS-based NCs translated into DNA damage (Figures 7 and 8) and alterations in cell cycle distribution (Figure 10). Our findings indicate that variations in polyelectrolyte composition influence not only uptake efficiency but also cellular responses to drug-loaded NCs, which may have important implications for the design and selection of NCs in targeted drug delivery strategies.

One of the key considerations in comparing the cytotoxicity of anticancer agents is determining the mode of intracellular transport by which the compounds are delivered into tumour tissue. It has previously been reported that free PTX enters cells predominantly via passive diffusion.[48] As a lipophilic molecule, PTX traverses the lipid bilayer of the plasma cell membrane and binds with high affinity to the β-subunit of tubulin within microtubules. This interaction stabilizes microtubules, thereby preventing the dynamic cytoskeleton reorganization required for mitosis. Stabilized microtubules are unable to depolymerize, resulting in mitotic arrest at the G2/M phase of the cell cycle, which ultimately leads to apoptosis over time. A primary limitation of PTX administration in clinical settings is its poor aqueous solubility and high binding affinity for human plasma proteins. Although the clinically approved formulation Taxol® - a micellar preparation of PTX using the surfactant Cremophor EL, enabling its systemic use, is associated with the occurrence of severe hypersensitivity reactions, as well as nephrotoxicity and neurotoxicity.[49] Comparative studies of Taxol and Abraxane® (an albumin-bound form of PTX) demonstrated that Abraxane exhibits superior cellular uptake, likely due to its internalization via gp60 receptor- and caveolae-mediated transcytosis.[50] Despite eliminating Cremophor EL, Abraxane still induces peripheral neuropathy and is cleared from circulation more rapidly than PEGylated or stealth nanoparticle-based formulations.[51]

Liposomal and polymeric micelle-based formulations are the main promising nanocarriers for PTX delivery, each offering distinct advantages.[52] Liposomes, composed of phospholipid bilayers, encapsulate PTX within their aqueous core or lipid bilayer, enhancing solubility and reducing systemic toxicity.[53] In contrast, polymeric micelles, formed by the self-assembly of amphiphilic block copolymers, provide superior drug loading capacity and stability, with the added benefit of tunable release profiles and potential for stimuli-responsive behavior.[54] Despite their promise as nanocarriers for PTX, neither liposomes nor polymeric micelles' clinical application can be classified as global. This occurs because liposomes frequently experience premature drug leakage, limited physical stability, and difficulties in large-scale manufacturing and reproducibility. Additionally, their relatively large size and susceptibility to rapid clearance by the mononuclear phagocyte system can compromise tumor accumulation and therapeutic efficacy.[55,56] On the other hand, polymeric micelles show low stability in vivo, with a tendency to dissociate upon dilution below the critical micelle concentration and premature drug release.[57] These drawbacks underscore the need for continued innovation in nanocarrier engineering to fully control the delivery route of PTX.

In this study, we proposed a novel DDS for PTX based on SDS-derived NCs, synthesised using the LbL technique and additionally labelled with RhoB. Upon physicochemical characterisation of the NCs, we found that the type of polyelectrolyte used during synthesis had a substantial impact on the zeta potential of the resulting nanoformulation. SDS/PLL NCs (with or without PTX and/or RhoB) exhibited a positive zeta potential. In contrast, the addition of an outer PGA layer reversed the surface charge, resulting in a negatively charged SDS/PLL/PGA complex.

The surface charge of NPs is a critical factor influencing the interactions between NPs and the cellular membrane. Cationic (positively charged) particles are known to exhibit strong electrostatic attraction to the negatively charged cell surface, thereby enhancing cellular uptake.[58] In contrast, the anionic NPs typically display reduced efficiency of cellular uptake due to electrostatic repulsion with components of the outer cell membrane. Furthermore, the surface charge of NPs also affects the internalization pathway by which NPs are taken up by cells.[59] Most drug-loaded NPs are internalized via endocytic mechanisms, which vary in complexity and specificity. These include several distinct routes, among which dynamin-dependent and -independent, as well as clathrin-mediated and clathrin-independent pathways, are the most widely recognized.[34,60]

Cationic NPs are frequently internalized by CME or macropinocytosis, whereas anionic or neutral nanocompounds tend to favor caveolae-mediated endocytosis.[61] In our study, cellular uptake of SDS-based NCs revealed that the

internalization route depends on the polyelectrolyte composition. Specifically, PGA-free SDS/PLL NCs are taken up primarily through dynamin-dependent endocytosis. At the same time, both SDS/PLL and SDS/PLL/PGA NCs utilize macropinocytosis as a primary route of entry.

Several studies have demonstrated that receptor-mediated endocytosis offers an efficient uptake mechanism and that ligand-receptor interactions can significantly enhance the in vitro antitumor efficacy of DDS compared to free drug administration. For example, Wang et al[62] reported that PTX conjugated with the tumour-targeting peptide A7R and the cell-penetrating peptide TAT facilitated receptor-mediated internalization by binding to Neuropilin-1, a key receptor involved in tumour angiogenesis. Another widely studied approach for targeted PTX delivery involves folate receptor-mediated endocytosis, using protein-based nanoparticle systems.[63]

Although ligand-coated NPs offer promise in nanomedicine, passive targeting remains a more robust, reproducible, and scalable approach, particularly in the context of heterogeneous and immunologically complex tumour microenvironments.[64] For example, cancer cells within the same tumour or across different patients may express target receptors at varying levels.[9] Drug delivery nanosystems that do not rely on ligands confer three principal advantages over actively targeted NPs: (1) they circumvent challenges related to tumour heterogeneity; (2) they can potentially reach all cancer cells exhibiting leaky vasculature, irrespective of receptor expression profiles; and (3) they eliminate the risk of reduced receptor's expression or its saturation, which over time may weaken the effectiveness of active targeting.[9] Consequently, the majority of clinically approved nanochemotherapeutics employ passive targeting strategies – for instance, liposomal doxorubicin [44] and albumin-bound PTX.[65]

Interestingly, our findings revealed that the differences in the uptake mechanisms of SDS-based NCs corresponded not only to their surface charge but also to their particle size. By employing a broad panel of endocytosis inhibitors, we demonstrated that dynamin-dependent uptake was essential exclusively for SDS/PLL NCs. In contrast, increasing the capsule diameter to approximately 110 nm, achieved by the addition of a PGA layer, favored macropinocytosis as the predominant route of internalization. Numerous studies have shown that NPs within the size range of 50–200 nm are generally optimal for endocytic uptake.[34] Notably, polymeric PTX NPs smaller than 100 nm are typically internalized via CME, whereas PTX-loaded liposomes more commonly engage macropinocytosis and clathrin-independent pathways with diameters of approximately 150 nm.[66]

Conversely, no significant differences in the uptake of SDS-based NCs were observed across the examined cell lines in our study, despite numerous reports highlighting distinct endocytic profiles between endothelial, epithelial, and mesenchymal-like cells.[67] These differences have been attributed to variations in membrane composition,[68] receptor expression,[69] and cytoskeletal organization.[70] Interestingly, when comparing the sensitivity of MCF-7, MDA-MB-231, and HMEC-1 cell lines assessed via ATP content and protein synthesis assays, we found that endothelial cells were more resistant to SDS/PLL/PTX and SDS/PLL/PGA/PTX than to the free drug. A similar phenomenon was observed in our analysis of cardiac cells, where HL-1 cardiomyocytes displayed the highest resistance to SDS/PLL/PGA/PTX among the tested formulations.[20]

What accounts for the observed differences in cytotoxicity between the examined PTX formulations? Firstly, we propose that free PTX, as a small and lipophilic molecule, is capable of passively diffusing across endothelial cell membranes and rapidly reaching intracellular targets such as tubulin, as previously demonstrated by Fellner et al.[71] In contrast, BC cells are generally more endocytically active due to their elevated metabolic rates. Therefore, even if similar uptake pathways are engaged, the rate and extent of NCs internalization may be lower in endothelial cells, limiting the intracellular release of PTX. Moreover, the release of PTX from NCs is often gradual, even when the mode of uptake (eg, CME) appears comparable in microscopy or inhibitor-based studies. While this controlled release profile is advantageous for tumour targeting, it may result in lower peak drug concentrations in non-target cells such as endothelial cells, thereby reducing cytotoxic effects.[58]

By relating the cytotoxic properties of PTX encapsulated in SDS-based NCs to our previous and current findings, we demonstrated that in BC cell lines, DNA damage induced by free PTX was comparable to that triggered by PTX-loaded SDS-based NCs in both MCF-7 and MDA-MB-231 cells. Even though some statistical changes were observed in the comet assay, we did not see a difference higher than 10% between PTX alone and the drug encapsulated in SDS/PLL or SDS/PLL/PGA (Figure 7). From a regulatory standpoint, genotoxicity assessment requires a battery of assays targeting

diverse endpoints, as no single method can detect all forms of DNA lesions. Phosphorylation of γH2AX at serine 139, forming γH2AX, plays a key role in the DNA damage response, particularly in the repair of double-strand breaks, thereby contributing to the survival of cancer cells. Upon DNA damage, γH2AX marks the site of the lesion and facilitates the recruitment of DNA repair proteins, orchestrating a complex repair process that includes activation of cell cycle checkpoints.[72] Although γH2AX is widely recognized as a biomarker of DNA damage in both research and clinical contexts,[73] pharmacological inhibition of its phosphorylation has emerged as a promising strategy to sensitize cancer cells to genotoxic therapies such as radiation and chemotherapy, thereby enhancing therapeutic efficacy.[74]

Regarding the genotoxic effect induced by nanoforms of PTX, our results are supported by findings in neuroblastoma SH-SY5Y cells, where DNA damage was observed after 24, 48, and 72 hours of exposure to poly(lactic-co-glycolic acid)-coated PTX NPs.[75] These DNA lesions also served as molecular markers of programmed cell death induced by SDS/PLL/PTX or SDS/PLL/PGA/PTX. For instance, our analyses revealed that the alteration in PARP activity was a direct consequence of G2/M phase arrest and the overexpression of kinases that regulate cell division. A comparable relationship was reported for PTX-loaded lipid nanocapsules (LNCs),[76] where PARP and caspase-3 cleavage provided clear evidence that LNCs functioned as effective DDS while retaining the pro-apoptotic activity of PTX in human BC cells.

In examining the genotoxic profiles of the tested NCs, a critical question arises regarding a potential mechanistic link between their cellular uptake pathways and the observed genotoxic effects. Indeed, the route of cellular internalization can influence the intracellular fate of nanocarriers and their interaction with organelles, including the nucleus. Dynamin-dependent endocytosis often leads to trafficking through endosomes and lysosomes, where acidic environments and enzymatic activity can destabilize nanocarriers, potentially releasing the drug prematurely or generating reactive molecules.[77] In contrast, dynamin-independent uptake (eg, caveolae-mediated or macropinocytosis) may bypass lysosomal degradation, leading to more controlled intracellular release and reduced exposure of sensitive organelles to toxic intermediates.[78] Finally, the physicochemical parameters, such as surface chemistry and charge distribution of the NCs, influence protein corona formation[79,80] membrane interaction, and intracellular trafficking, all of which can modulate genotoxic consequences.

Conclusion

Our findings suggest that the uptake mechanism of SDS-based NCs and their genotoxicity are not independent phenomena. The variations in the composition of polyelectrolytes used during the LbL synthesis of SDS-based NCs exert markedly different effects on the cytotoxic and genotoxic profiles of PTX delivered via these nanosystems. These differences are critically important, as they influence both the mode of endocytosis involved in the uptake of SDS/PLL and SDS/PLL/PGA NCs, as well as the stability of the cellular genome. While the current study provides important insights into the genotoxic outcomes and uptake mechanisms of the tested NCs in vitro, future in vivo studies are planned to assess their translational relevance in a physiological context.

Abbreviations

ATCC, American Type Culture Collection; ATM, Ataxia-telangiectasia mutated; ATR, ATM and Rad3-related; BC, breast cancer; BCA, bicinchoninic acid; Cdc42, cell division control protein 42 homolog; CDK1, Cyclin-dependent kinase 1; CME, clathrin-mediated endocytosis; CLIC, clathrin-independent carriers; DAPI, 4′,6-diamidino-2-phenylindole; DDS, drug delivery systems; DMEM, Dulbecco's Modified Eagle Medium; EGF, epidermal growth factor; EIPA, 5-(N-ethyl-N-isopropyl)amiloride; ELISA, Enzyme-linked immunosorbent assay; FBS, fetal bovine serum; FEME, endophilin-mediated endocytosis; GEEC, glycosylphosphatidylinositol-anchored protein-enriched endosomal compartment; γH2AX, H2A histone family member X; HMBS, Hydroxymethylbilane synthase; HMEC-1, dermal microvascular endothelial cell line; HPRT1, Hypoxanthine phosphoribosyltransferase; H_2O_2, hydrogen peroxide; LbL, Layer-by-Layer; LNCs, lipid nanocapsules; MCF-7, epithelial breast adenocarcinoma cell line; MDA-MB-231, triple-negative, mesenchymal-like breast cancer cell line; NaCl, sodium chloride; NCs, nanocarriers; NPs, nanoparticles; PDI, polydispersity index; PBS, phosphate-buffered saline; PE, phycoerythrin; PGA, poly-L-glutamic acid; PI, propidium iodide; PI3K, phosphoinositide 3-kinase; PLL, poly-L-lysine; PLL/RhoB, rhodamine-labelled poly-L-lysine; PTX, paclitaxel; PARP, Poly(ADP-ribose) polymerase; RhoA, Ras homolog family member A; qRT-PCR —quantitative real-time reverse

transcription polymerase chain reaction; RhoB, Rhodamine B; RPMI, Roswell Park Memorial Institute; SDS, sodium dodecyl sulphate.

Acknowledgments

The group in Lodz thanks Kacper Wiktorowski and Kamila Podsiadlo for technical assistance with the in vitro studies.

Funding

This research was funded by the National Science Centre (Poland) within the framework of the Miniatura program (grant number 2020/04/X/NZ3/00770) and partial funding from the GetSmarter Project at the Faculty of Biology and Environmental Protection, University of Lodz, Poland (edition 2022/23).

Disclosure

Marzena Szwed reports a patent PL 247686 licensed to University of Lodz. Agnieszka Marczak reports a patent (PL 247686) issued to Marzena Szwed, Agnieszka Marczak, Krzysztof Szczepanowicz. Krzysztof Szczepanowicz reports grants from National Science Centre, during the conduct of the study (grant number 2020/04/X/NZ3/00770); In addition, Dr Krzysztof Szczepanowicz has a patent PL 247686 issued. The authors report no other conflicts of interest in this work.

References

1. Bray F, Laversanne M, Sung HYA, et al. Global cancer statistics 2022: GLOBOCAN estimates of incidence and mortality worldwide for 36 cancers in 185 countries. *Ca*. 2024;74(3):229–263. doi:10.3322/caac.21834
2. Obidiro O, Battogtokh G, Akala EO. Triple negative breast cancer treatment options and limitations: future outlook. *Pharmaceutics*. 2023;15 (7):1796. doi:10.3390/pharmaceutics15071796
3. Xiong X, Zheng LW, Ding Y, et al. Breast cancer: pathogenesis and treatments. *Signal Transduction Tar*. 2025;10(1):49.
4. Mata DGDM, Rush MB, Smith-Uffen M, et al. The omission of anthracycline chemotherapy in women with early HER2-negative breast cancer-a systematic review and meta-analysis. *Curr Oncol*. 2024;31(8):4486–4506. doi:10.3390/curroncol31080335
5. Zeien J, Qiu W, Triay M, et al. Clinical implications of chemotherapeutic agent organ toxicity on perioperative care. *Biomed Pharmacother*. 2022;146:112503.
6. Ndongwe T, Zhou AA, Ganga NP, et al. The use of nanomaterials as drug delivery systems and anticancer agents in the treatment of triple-negative breast cancer: an updated review (year 2005 to date). *Discov Nano*. 2024;19(1). doi:10.1186/s11671-024-04089-3
7. Tewabe A, Abate A, Tamrie M, Seyfu A, Siraj EA. Targeted drug delivery - from magic bullet to nanomedicine: principles, challenges, and future perspectives. *J Multidiscip Health*. 2021;14:1711–1724. doi:10.2147/JMDH.S313968
8. Joseph TM, Mahapatra DK, Esmaeili A, et al. Nanoparticles: taking a unique position in medicine. *Nanomaterials*. 2023;13(3). doi:10.3390/nano13030574
9. Chehelgerdi M, Chehelgerdi M, Allela OQB, et al. Progressing nanotechnology to improve targeted cancer treatment: overcoming hurdles in its clinical implementation. *Mol Cancer*. 2023;22(1):169.
10. Fan DH, Cao YK, Cao MQ, Wang YJ, Cao YL, Gong T. Nanomedicine in cancer therapy. *Signal Transduction Tar*. 2023;8(1):293.
11. Wang BL, Hu SQ, Teng Y, et al. Current advance of nanotechnology in diagnosis and treatment for malignant tumors. *Signal Transduction Tar*. 2024;9(1):200.
12. Wu J. The Enhanced Permeability and Retention (EPR) effect: the significance of the concept and methods to enhance its application. *Journal of Personalized Medicine*. 2021;11(8):771. doi:10.3390/jpm11080771
13. Zhao LL, Skwarczynski M, Toth I. Polyelectrolyte-based platforms for the delivery of peptides and proteins. *Acs Biomater Sci Eng*. 2019;5 (10):4937–4950. doi:10.1021/acsbiomaterials.9b01135
14. Placci M, Giannotti MI, Muro S. Polymer-based drug delivery systems under investigation for enzyme replacement and other therapies of lysosomal storage disorders. *Adv Drug Deliv Rev*. 2023;197:114683.
15. Traeger A, Leiske MN. Challenges and perspectives in polyelectrolytes. *Biomacromolecules*. 2024;26(1):5–32. doi:10.1021/acs.biomac.4c01061
16. Ewii UE, Attama AA, Olorunsola EO, et al. Nanoparticles for drug delivery: insight into in vitro and in vivo drug release from nanomedicines. *Nano TransMed*. 2025;4:100083.
17. Ly PD, Ly KN, Phan HL, Nguyen HHT, Duong VA, Nguyen HV. Recent advances in surface decoration of nanoparticles in drug delivery. *Front Nanotechnol*. 2024;6:1456939.
18. Zhang MM, Gao S, Yang DJ, et al. Influencing factors and strategies of enhancing nanoparticles into tumors. *Acta Pharm Sin B*. 2021;11 (8):2265–2285. doi:10.1016/j.apsb.2021.03.033
19. Szwed M, Michlewska S, Kania K, Szczech M, Marczak A, Szczepanowicz K. New SDS-based polyelectrolyte multicore nanocarriers for paclitaxel delivery-synthesis, characterization, and activity against breast cancer cells. *Cells*. 2023;12(16):2052. doi:10.3390/cells12162052
20. Szwed M, Poczta-Krawczyk A, Kania KD, et al. Multicore, SDS-based polyelectrolyte nanocapsules as novel nanocarriers for paclitaxel to reduce cardiotoxicity by protecting the mitochondria. *Int J Mol Sci*. 2025;26(3):901. doi:10.3390/ijms26030901
21. Sukhorukov GB, Donath E, Lichtenfeld H, et al. Layer-by-layer self assembly of polyelectrolytes on colloidal particles. *Colloid Surf A*. 1998;137 (1–3):253–266. doi:10.1016/S0927-7757(98)00213-1
22. Bollhorst T, Rezwan K, Maas M. Colloidal capsules: nano- and microcapsules with colloidal particle shells. *Chem Soc Rev*. 2017;46(8):2091–2126. doi:10.1039/c6cs00632a

23. Pajor-Swierzy A, Szczepanowicz K, Kamyshny A, Magdassi S. Metallic core-shell nanoparticles for conductive coatings and printing. *Adv Colloid Interfac*. 2022;299:102578.
24. Hashemi M, Omidi M, Muralidharan B, et al. Layer-by-layer assembly of graphene oxide on thermosensitive liposomes for photo-chemotherapy. *Acta Biomater*. 2018;65:376–392. doi:10.1016/j.actbio.2017.10.040
25. Ivanov AS, Pershina LV, Nikolaev KG, Skorb EV. Recent progress of layer-by-layer assembly, free-standing film and hydrogel based on polyelectrolytes. *Macromol Biosci*. 2021;21(10). doi:10.1002/mabi.202100117
26. Gerasimovich E, Kriukova I, Shishkov VV, et al. Interaction of serum and plasma proteins with polyelectrolyte microparticles with core/shell and shell-only structures. *Acs Omega*. 2024;9(27):29739–29750. doi:10.1021/acsomega.4c03307
27. Navolokin N, Lomova M, Bucharskaya A, et al. Antitumor effects of microencapsulated extract on breast carcinoma and human cervical cancer cells in vitro. *Materials*. 2023;16(4):1470. doi:10.3390/ma16041470
28. Szczepanowicz K, Hoel HJ, Szyk-Warszynska L, et al. Formation of biocompatible nanocapsules with emulsion core and pegylated shell by polyelectrolyte multilayer adsorption. *Langmuir*. 2010;26(15):12592–12597. doi:10.1021/la102061s
29. Karabasz A, Bzowska M, Szczepanowicz K. Biomedical applications of multifunctional polymeric nanocarriers: a review of current literature. *Int J Nanomed*. 2020;15:8673–8696. doi:10.2147/IJN.S231477
30. Iversen TG, Skotland T, Sandvig K. Endocytosis and intracellular transport of nanoparticles: present knowledge and need for future studies. *Nano Today*. 2011;6(2):176–185. doi:10.1016/j.nantod.2011.02.003
31. Filippini A, D'Alessio A. Caveolae and lipid rafts in endothelium: valuable organelles for multiple functions. *Biomolecules*. 2020;10(9):1218. doi:10.3390/biom10091218
32. Qian XL, Pan YH, Huang QY, et al. Caveolin-1: a multifaceted driver of breast cancer progression and its application in clinical treatment. *Oncol Targets Ther*. 2019;12:1539–1552. doi:10.2147/OTT.S191317
33. Xiao JM, Zhao T, Fang WL, et al. Caveolin-1 signaling-driven mitochondrial fission and cytoskeleton remodeling promotes breast cancer migration. *Int J Biochem Cell B*. 2022;152:106307.
34. de Almeida MS, Susnik E, Drasler B, Taladriz-Blanco P, Petri-Fink A, Rothen-Rutishauser B. Understanding nanoparticle endocytosis to improve targeting strategies in nanomedicine. *Chem Soc Rev*. 2021;50(9):5397–5434.
35. Hermanson GT. *Bioconjugate Techniques, 3rd Edition*. 2013:1–1146.
36. Singh NP, McCoy MT, Tice RR, Schneider EL. A simple technique for quantitation of low levels of DNA damage in individual cells. *Exp Cell Res*. 1988;175(1):184–191. doi:10.1016/0014-4827(88)90265-0
37. Li GW, Burkhardt D, Gross C, Weissman JS. Quantifying absolute protein synthesis rates reveals principles underlying allocation of cellular resources. *Cell*. 2014;157(3):624–635. doi:10.1016/j.cell.2014.02.033
38. Sun YN, Zhou YX, Rehman M, Wang YF, Guo ST. Protein corona of nanoparticles: isolation and analysis. *Chem Bio Eng*. 2024;1(9):757–772. doi:10.1021/cbe.4c00105
39. Lamaze C, Tardif N, Dewulf M, Vassilopoulos S, Blouin CM. The caveolae dress code: structure and signaling. *Curr Opin Cell Biol*. 2017;47:117–125. doi:10.1016/j.ceb.2017.02.014
40. Manoli SS, Kisor K, Webb BA, Barber DL. Ethyl isopropyl amiloride decreases oxidative phosphorylation and increases mitochondrial fusion in clonal untransformed and cancer cells. *Am J Physiol*. 2021;321(1):C147–C157. doi:10.1152/ajpcell.00001.2021
41. Bianchini A, Wood CM. Potency and specificity of amiloride and its analogues on branchial sodium fluxes in freshwater trout and goldfish. *Comp Biochem Phys A*. 2024;297:111715.
42. Lim HS, Lee MY, Moon JS, et al. Actin cytoskeleton and golgi involvement in movement and cell wall localization of triple gene block proteins. *Plant Pathology J*. 2013;29(1):17–30. doi:10.5423/PPJ.OA.09.2012.0144
43. Hansen SH, Olsson A, Casanova JE. Wortmannin, an inhibitor of phosphoinositide 3-kinase, inhibits transcytosis in polarized epithelial cells. *J Biol Chem*. 1995;270(47):28425–28432. doi:10.1074/jbc.270.47.28425
44. He ZW, Xia BH, Zhao TQ, et al. Clathrin-independent carriers/glycosylphosphatidylinositol-anchored-protein-enriched endosomal compartment endocytic pathway is critical for enterovirus A71 entry into human oral epidermoid carcinoma KB cells. *J Med Virol*. 2025;97(5). doi:10.1002/jmv.70369
45. Demir E, Qin T, Li Y, et al. Cytotoxicity and genotoxicity of cadmium oxide nanoparticles evaluated using in vitro assays. *Mutat Res Genet Toxicol Environ Mutagen*. 2020;850:503149. doi:10.1016/j.mrgentox.2020.503149
46. Dunkenberger L, Reiss K, Del Valle L. Comet assay for the detection of single and double-strand DNA breaks. *Methods Mol Biol*. 2022;2422:263–269.
47. Lavin MF, Delia D, Chessa L. ATM and the DNA damage response - Workshop on ataxia-telangiectasia and related syndromes. *EMBO Rep*. 2006;7(2):154–160. doi:10.1038/sj.embor.7400629
48. Muley H, Fadó R, Rodríguez-Rodríguez R, Casals N. Drug uptake-based chemoresistance in breast cancer treatment. *Biochem. Pharmacol*. 2020;177:113959.
49. Irizarry LD, Luu TH, McKoy JM, et al. Cremophor EL-containing paclitaxel-induced anaphylaxis: a call to action. *Community Oncol*. 2009;6(3):132–134. doi:10.1016/S1548-5315(11)70224-8
50. Murphy G, Brayden DJ, Cheung DL, Liew A, Fitzgerald M, Pandit A. Albumin-based delivery systems: recent advances, challenges, and opportunities. *J Control Release*. 2025;380:375–395. doi:10.1016/j.jconrel.2025.01.035
51. Deng X, Huang X, Dong X, Mao G, Xing W. Efficacy and safety of nanopaclitaxel formulation for cancer treatment: evidence from randomized clinical trials. *Nanomedicine*. 2023;18(10):833–843. doi:10.2217/nnm-2023-0080
52. Noori A, Salehi Namini M, Azaryan E, Ataei M, Beheshtizadeh N. Nanofibers for paclitaxel delivery: a promising avenue for cancer therapy. *Biomed Pharmacother*. 2025;192:118607. doi:10.1016/j.biopha.2025.118607
53. Yang T, Cui FD, Choi MK, et al. Liposome formulation of paclitaxel with enhanced solubility and stability. *Drug Deliv*. 2007;14(5):301–308. doi:10.1080/10717540601098799
54. Zhou M, Wen LJ, Wang C, Lei Q, Li YX, Yi XQ. Recent advances in stimuli-sensitive amphiphilic polymer-paclitaxel prodrugs. *Front Bioeng Biotech*. 2022;10:875034.
55. Chelliah R, Rubab M, Vijayalakshmi S, Karuvelan M, Barathikannan K, Oh D-H. Liposomes for drug delivery: classification, therapeutic applications, and limitations. *Next Nanotechnol*. 2025;8:100209. doi:10.1016/j.nxnano.2025.100209

56. Choudhury A, Kirti A, Lenka SS, et al. Strategic advances in liposomes technology: translational paradigm in transdermal delivery for skin dermatosis. *J Nanobiotechnol*. 2025;23(1):576.
57. Negut I, Bita B. Polymeric micellar systems-a special emphasis on "smart" drug delivery. *Pharmaceutics*. 2023;15(3):976. doi:10.3390/pharmaceutics15030976
58. Behzadi S, Serpooshan V, Tao W, et al. Cellular uptake of nanoparticles: journey inside the cell. *Chem Soc Rev*. 2017;46(14):4218–4244. doi:10.1039/C6CS00636A
59. Balog S, de Almeida MS, Taladriz-Blanco P, Rothen-Rutishauser B, Petri-Fink A. Does the surface charge of the nanoparticles drive nanoparticle-cell membrane interactions? *Curr Opin Biotech*. 2024;87:103128.
60. Salatin S, Khosroushahi AY. Overviews on the cellular uptake mechanism of polysaccharide colloidal nanoparticles. *J Cell Mol Med*. 2017;21(9):1668–1686. doi:10.1111/jcmm.13110
61. Mazumdar S, Chitkara D, Mittal A. Exploration and insights into the cellular internalization and intracellular fate of amphiphilic polymeric nanocarriers. *Acta Pharm Sin B*. 2021;11(4):903–924. doi:10.1016/j.apsb.2021.02.019
62. Wang LK, Zhao CQ, Lu L, Jiang HL, Wang FS, Zhang XK. Transcytosable peptide-paclitaxel prodrug nanoparticle for targeted treatment of triple-negative breast cancer. *Int J Mol Sci*. 2023;24(5):4646.
63. Soe ZC, Ou WQ, Gautam M, et al. Development of folate-functionalized PEGylated zein nanoparticles for ligand-directed delivery of paclitaxel. *Pharmaceutics*. 2019;11(11):562. doi:10.3390/pharmaceutics11110562
64. Abdullah KM, Sharma G, Singh AP, Siddiqui JA. Nanomedicine in cancer therapeutics: current perspectives from bench to bedside. *Mol Cancer*. 2025;24(1). doi:10.1186/s12943-025-02368-w
65. Harshita, Barkat MA, Beg S, Pottoo FH, Ahmad FJ, Ahmad FJ. Nanopaclitaxel therapy: an evidence based review on the battle for next-generation formulation challenges. *Nanomedicine*. 2019;14(10):1323–1341. doi:10.2217/nnm-2018-0313
66. Xing YB, Lian XJ, Zhang YR, Zhang YL, Guo XH. Polymeric liposomes targeting dual transporters for highly efficient oral delivery of paclitaxel. *Carbohyd Polym*. 2024;334.
67. Ribatti D. Epithelial-endothelial transition and endothelial-mesenchymal transition. *Int J Dev Biol*. 2022;66(4–6):311–316. doi:10.1387/ijdb.210234dr
68. Cupic KI, Rennick JJ, Johnston APR, Such GK. Controlling endosomal escape using nanoparticle composition: current progress and future perspectives. *Nanomedicine*. 2019;14(2):215–223. doi:10.2217/nnm-2018-0326
69. De Schutter E, Ramon J, Pfeuty B, et al. Plasma membrane perforation by GSDME during apoptosis-driven secondary necrosis. *Cell. Mol. Life Sci*. 2022;79(1). doi:10.1007/s00018-021-04078-0
70. Katrukha EA, Mikhaylova M, van Brakel HX, et al. Probing cytoskeletal modulation of passive and active intracellular dynamics using nanobody-functionalized quantum dots. *Nat Commun*. 2017;8(1):8. doi:10.1038/s41467-017-00021-9
71. Fellner S, Bauer B, Miller DS, et al. Transport of paclitaxel (Taxol) across the blood-brain barrier in vitro and in vivo. *J Clin Invest*. 2002;110(9):1309–1318. doi:10.1172/JCI0215451
72. Podhorecka M, Skladanowski A, Bozko P. H2AX phosphorylation: its role in DNA damage response and cancer therapy. *J Nucleic Acids*. 2010;2010. doi:10.4061/2010/920161
73. Rahmanian N, Shokrzadeh M, Eskandani M. Recent advances in γH2AX biomarker-based genotoxicity assays: a marker of DNA damage and repair. *DNA Repair*. 2021;108:103243. doi:10.1016/j.dnarep.2021.103243
74. Prabhu KS, Kuttikrishnan S, Ahmad N, et al. H2AX: a key player in DNA damage response and a promising target for cancer therapy. *Biomed Pharmacother*. 2024;175:116663.
75. Bacanli M, Esim Ö, Erdogan H, Sarper M, Erdem O, Özkan Y. Evaluation of cytotoxic and genotoxic effects of paclitaxel-loaded PLGA nanoparticles in neuroblastoma cells. *Food Chem Toxicol*. 2021;154:112323.
76. Valsalakumari R, Yadava SK, Szwed M, et al. Mechanism of cellular uptake and cytotoxicity of paclitaxel loaded lipid nanocapsules in breast cancer cells. *Int J Pharmaceut*. 2021;597:120217.
77. Desai N, Rana D, Salave S, Benival D, Khunt D, Prajapati BG. Achieving endo/lysosomal escape using smart nanosystems for efficient cellular delivery. *Molecules*. 2024;29(13):3131. doi:10.3390/molecules29133131
78. Butt AM, Abdullah N, Rani NNIM, Ahmad N, Amin MCIM. Endosomal escape of bioactives deployed nanocarriers: insights into the design of polymeric micelles. *Pharm Res-Dordr*. 2022;39(6):1047–1064. doi:10.1007/s11095-022-03296-w
79. Moscatiello GY, Natale C, Inserra M, et al. The surface charge both influences the penetration and safety of polystyrene nanoparticles despite the protein corona formation. *Environ Sci-Nano*. 2025;12(5):2857–2870. doi:10.1039/D4EN00962B
80. Bilardo R, Traldi F, Vdovchenko A, Resmini M. Influence of surface chemistry and morphology of nanoparticles on protein corona formation. *Wires Nanomed Nanobi*. 2022;14(4). doi:10.1002/wnan.1788